

Autopresentation

Dr Katarzyna Małgorzata Rećko

Białystok 2016

“It is only slightly overstating the case to say that physics is the study of symmetry”

P. W. Anderson[1ⁱ]

To My Beloved Daughters

Ad 1.¹.

Katarzyna Rećko

Ad 2.

The degree Master of Science in Chemistry obtained at the Faculty of Mathematics - natural sciences, Warsaw University Branch in Białystok, 07.10.1993; Thesis: "Models of the hydrogen bonds in the crystallochemistry" under the guidance of prof. dr hab. Sławomir Grabowski

Ph.D. - physical sciences in Physics obtained at the Faculty of Mathematics - Physics University of Białystok, 8.10.2003; Dissertation: "Research of the properties of the crystal and magnetic structures of A-Fe-Al (A = U, Th, Sc) alloys of ThMn₁₂ type structure" under the guidance of prof. dr hab. Ludwik Dobrzyński

Ad 3.

1993 – 1995 Assistant of the Institute of Chemistry, Warsaw University Branch in Białystok

1995 – 1997 Assistant of the Institute of Experimental Physics, Warsaw University Branch in Białystok

1997 – 2004 Assistant of Institute of Physics, University of Białystok

2004 – 2008 Adiunct of Institute of Physics, University of Białystok

2008 – Adiunct of Faculty of Physics, University of Białystok

Ad 4.²:

a)

Magnetic structure and basic interactions of MFe₄Al₈ (M=Sc and U)

b)

The results of investigations were described in the following papers abbreviated by appropriate acronym H:

| Ac. | Bibliographic data and Personal contribution to the collaborative scientific work | Cit. | IF | Person. Contrib. % |
|-----|---|------|------|--------------------------|
| H1 | K. Rećko , B. C. Hauback, L. Dobrzyński, K. Szymański, D. Satuła, B. Yu. Kotur, W. Suski, Modulated Magnetic Structure of ScFe ₄ Al ₈ by X-ray, Neutron Powder Diffraction and Mössbauer Effect, Journal of Magnetism and Magnetic Materials 272-276 (2004) 764-766 I performed and interpreted X-ray powder diffraction measurements. The neutron diffraction experiments were | 1 | 1.97 | 70 |

¹ Przygotowano według wzoru (http://www.ck.gov.pl/images/PDF/komunikaty/wzor_wniosku.pdf)

² Wskazanie osiągnięcia* wynikającego z art. 16 ust. 2 ustawy z dnia 14 marca 2003 r. o stopniach naukowych i tytule naukowym oraz o stopniach i tytule w zakresie sztuki (Dz. U. nr 65, poz. 595 ze zm.)

| | | | | |
|----|---|---|------|----|
| | performed by B.C. Hauback. I worked on the interpretation of the neutron data i. e. I suggested the models and did the refinements of the magnetic structures. I assisted in the collection and I collaborated in interpretation of the Mössbauer data. The samples were prepared by the other authors. | | | |
| H2 | K. Rećko , L. Dobrzyński, A. Goukassov, M. Biernacka, M. Brancewicz, A. Makal, K. Woźniak, J. Waliszewski, E. Talik, B. Yu. Kotur, W. Suski, Magnetic phase transitions in ScFe ₄ Al ₈ by powder and single crystal neutron diffraction, Phase Transitions (2007) Vol. 80, Nos 6-7, 575-586 I carried out the diffraction powder and single crystal measurements and data interpreted. The neutron diffraction I did in close collaboration with A. Goukassov. I took part in the Mössbauer and magnetization measurements on the planning stage of temperature and external magnetic field scenario. | 6 | 0.95 | 70 |
| H3 | K. Rećko , L. Dobrzyński, A. Goukassov, M. Biernacka, M. Brancewicz, A. Makal, K. Woźniak, J. Waliszewski, E. Talik, B. Yu. Kotur, W. Suski, Magnetic phase transitions in ScFe ₄ Al ₈ , Complementary Methods in the Investigations of the Condensed Phases, Publisher: University of Podlasie 1 (2008) 131-146 My part to this work concerned the collection and interpretation of the diffraction data and the collaboration during the Mössbauer and magnetization measurements. I was responsible for the review of available literature concerning the magnetic structures of ThMn ₁₂ compounds and collected in the framework of my PhD thesis. | - | - | 70 |
| H4 | K. Rećko , L. Dobrzyński, M.-H. Lemée - Cailleau, J. Waliszewski, E. Talik, W. Suski and P. Courtois, On the Crystal and Magnetic Behaviour of ScFe ₄ Al ₈ Single Crystal, Acta Physica Polonica A 115 (2009) 206-208 I performed and interpreted X-ray powder diffraction measurements. The neutron experiments were performed in close collaboration by me and M.-H. Lemée - Cailleau. I took the initiative to use hard X-ray scattering and I was responsible for the group symmetry analysis and deciphering of a crystal structure doubling as well. A complementary experiment by use hard X-ray diffraction was done by P. Courtois. | 3 | 0.53 | 80 |
| H5 | K. Rećko , L. Dobrzyński, A. Senyshyn, H. Fuess, K. Szymański, B. Yu. Kotur, W. Suski, Structural and magnetic properties of Sc _{1.1} Fe _{3.9} Al ₈ , Journal of Magnetism and Magnetic Materials 323 (2011) 1860 -1867 I assisted in the sample preparation and performed the thermal samples treatment. The main part of the neutron diffraction experiments were done in close collaboration by me and A. Senyshyn. The data analysis concerning the X-ray and neutron experiments was done by me. I assisted in the Mössbauer Spectroscopy and magnetization measurements. | 2 | 1.97 | 80 |
| H6 | K. Rećko , L. Dobrzyński, J. Waliszewski, K. Szymański, Magnetic anisotropy in the incommensurate ScFe ₄ Al ₈ system, Journal of Magnetism and Magnetic Materials 388 (2015) 82-89 It was a challenge for me to use MCMag and MCPhase program packages to do the calculation of exchange integrals with the option to take into account different mechanisms. I constructed | 1 | 1.97 | 80 |

| | | | | |
|----|---|---|------|-----|
| | the model analysis based on an anisotropic bilinear two-ion exchange interaction. I reconciled Monte Carlo calculations with single crystal neutron and magnetization data. | | | |
| H7 | K. Rećko , L. Dobrzyński, J. Waliszewski, K. Szymański, Reconstruction of the Exchange Integrals Map of ScFe_4Al_8 Magnetic Structure, Acta Physica Polonica A 127 (2015) 424-426 I constructed the model analysis of the exchange interactions by use different MC program packages with the option to take into account Dzyaloshinskii – Moriya common with and without <i>RKKY</i> exchange mechanism and I reconciled calculations with single crystal neutron data. | - | 0.53 | 80 |
| H8 | K. Rećko , Exchange Integrals of Commensurate and Incommensurate Structures of MFe_4Al_8 ($M = \text{U, Sc}$), Journal of Optoelectronic and Advanced Materials, Vol. 17, No. 9-10 (2015) 1403-1409 I constructed the model analysis of the exchange interactions by use <i>McMag</i> and <i>McPhase</i> program packages with the option to take into account <i>RKKY</i> with bilinear two-ion exchange interactions tensors and I reconciled calculations with single crystal neutron data. | - | 0.43 | 100 |
| H9 | J. Waliszewski, K. Rećko , Magnetization distribution in noncollinear magnetic systems with mutually perpendicular crystal axes, Journal of Optoelectronics and Advanced Materials Vol. 17, No.7-8 (2015) 958-962 The vectorial magnetization distribution by use Maximum Entropy Method (<i>MEM</i>) was invented and calculated by J. Waliszewski. I was responsible for the preparation of the input data required by <i>MEM</i> , starting from my own detailed description of magnetic system in question. | - | 0.43 | 30 |

c)

(i) *The aim of the research presented here was to uncover the specific mechanisms leading to frequently noncollinear and incommensurate magnetic ordering of the alloys based on metals with the localized magnetic moments, i.e. the elements of so-called 3d block coupled through band electrons as for example in light Actinides – 5f.*

(ii) *The intention of the Authors was also the comparison of obtained experimental results relating to research the magnetic properties of MFe_4Al_8 ($M = f$ - elements, Sc) systems in the context of documented properties of the other members of this family.*

(iii) *Presented analysis relates to noncollinear and/or incommensurate magnetic structures revealed under conditions of weak diffraction intensities.*

TABLE OF CONTENTS

| | | |
|-----|--|----|
| 1 | Preface and publication guide..... | 6 |
| 2 | Modulated magnetic structure of ScFe_4Al_8 by X-ray, neutron powder diffraction and Mössbauer effect [H1]..... | 9 |
| 3 | Magnetic phase transitions in ScFe_4Al_8 by powder and single crystal neutron diffraction [H2]..... | 11 |
| 4 | Magnetic phase transitions in ScFe_4Al_8 [H3]..... | 17 |
| 5 | On the crystal and magnetic behaviour of ScFe_4Al_8 single crystal [H4]..... | 21 |
| 6 | Structural and magnetic properties of $\text{Sc}_{1.1}\text{Fe}_{3.9}\text{Al}_8$ [H5]..... | 31 |
| 7 | Magnetic anisotropy in the incommensurate ScFe_4Al_8 system [H6]..... | 33 |
| 7.1 | Direct exchange..... | 34 |
| 7.2 | RKKY interactions..... | 34 |
| 7.3 | Anisotropic exchange..... | 35 |
| 7.4 | Crystal field and anisotropy in terms of the Monte Carlo methods..... | 36 |
| 8 | Reconstruction of the exchange integrals map of ScFe_4Al_8 magnetic structure [H7]..... | 45 |
| 9 | Exchange integrals of commensurate and incommensurate structures of MFe_4Al_8 ($\text{M} = \text{U}, \text{Sc}$) [H8]..... | 47 |
| 10 | Magnetization distribution in noncollinear magnetic systems with mutually perpendicular crystal axes [H9]..... | 51 |
| 11 | Main achievements..... | 53 |

1 PREFACE AND PUBLICATION GUIDE

Physics of transition metals and physics of f -electron elements belong to permanently fascinating subject. The experimental and theoretical research groups are interested in the mechanisms of fundamental interactions between atoms, leading to the formation of a specific crystal structures, the conditions for the formation of magnetic moments in metals and basic interactions between magnetic moments in the conditions of metallic bonds. The importance of the symmetry as well as the nature of the magnetic interactions between even distant

partners are discussed and illustrated by selected systems. The correlation between the alloy's composition and their degree of order are taken into consideration.

The aim of the research presented here was to uncover the specific mechanisms leading to frequently noncolinear and incommensurate magnetic ordering of the alloys based on metals with the typical localized magnetic moments, i.e. the elements of so-called *3d* block coupled through band electrons as for example in light Actinides – *5f*.

The first quoted paper [H1] concerns the studies on which the theses and conclusions contained in this habilitation work were based. Although it is clear now that they could have finalized my PhD dissertation, this was not possible before accumulating new information. The paper mentioned above opened completely new chapter in the search for the mechanisms responsible for long-range magnetic ordering of intermetallic systems based on simple *p*- and *d*-electron metals, in which, after all there is no dominance of effects such as magnetocrystalline anisotropy. For this reason, main attention was devoted to the aspects of symmetry of periodic commensurate crystal structures as well as commensurate and incommensurate magnetic ones. For the sake of clarity, a brief overview of known mechanisms of direct, indirect and super- exchange interactions of the Fe atoms, which have in the neighborhood *p*, *d* or *f*-electrons is given together with the general review of elementary sources of anisotropy due to the components of the measured compounds.

In the paper mentioned above [H1] research of well-ordered single crystal of ScFe_4Al_8 showed unexpectedly two phase transition temperatures and two magnetic modulation vectors [H2]. Purely classical studies of the commensurate spin-canted and incommensurate magnetic structures in the same crystal symmetry were published in a Polish monograph [H3]. The observed, quite unusual and very complex magnetic ordering of the compounds crystallizing in a ThMn_{12} -type structure, which are finally purely intermetallic alloys, forced the necessity of carrying out an analysis using the irreducible representation of magnetic groups. Reduction of the symmetry seemed rational and was offering a possibility of explaining magnetic coupling observed in the light of the experimental results. The results obtained for seemingly least complicated iron's nearest neighbor, namely scandium, thus least complex spin rearrangement, demonstrated however the existence of two different modes observed in the neutron magnetic scattering. The diffraction pattern revealed eight reflections of the satellites around the reflections of nuclear type $(2n + 1, 2n + 1, 2n)$, and only four satellites around $(2n, 2n, 2n)$ ones. It remained an open question, in which coordination zones – the first or both first and second – iron tends to break its expected collinear magnetic order. Furthermore, the limited range of magnetic interactions up to such two zones, distinguished according to the criteria described in details in paper [H3] forced to careful consideration of magnetic superexchange interactions. Noteworthy, the first zone belongs to the iron neighbors distant by $\sim 2.5 \text{ \AA}$ and more distant “nonmagnetic” aluminum atoms. The second zone is exclusively occupied by scandium neighbors at a distance of 3.3 \AA , while the second magnetic neighbors

(third zone) are away by a distance over 4.3 Å (Table 1 of paper H3). During investigations of aforementioned satellites with help of the Laue camera - instrument Vivaldi (ILL, Grenoble) making use of the continuous spectrum of the penetrating neutron beam - further ambiguities related to the crystal structure have been detected [H4]. High temperature laueograms revealed the presence of many new spots fulfilling the extinction rule $h + k + l = 2n$, but in 4-times ($2a \times a \times 2c$) or 8-times $2(a \times a \times c)$ larger crystal unit cell. It was natural to suspect that chemical composition of the crystal could be responsible for the observed effect. Thus a series of $\text{Sc}_{1+x}\text{Fe}_{4-x}\text{Al}_8$ alloys was prepared for further studies. The sample of relatively good quality, showing a trace of $\text{Fe}_4\text{Al}_{13}$ only, was $x=0.1$ [H5]. It is worth noting that in the above mentioned systems, it is aluminum – relatively large atom – which is stabilizing the crystal structure.

All of the presented papers concern the results of experiments performed with the use of non-polarized neutron beams in the scenario of elastic and coherent scattering. Analysis of data collected for high symmetry directions allow determination of the details of magnetic interactions [H6] - of exchange constants derived within the Weiss' molecular field theory approximation of the crystal field or in the tensor resulting from a search of the exchange constants by Monte Carlo methods [H6]. Recent papers in this vein [H7, H8, H9] are trying to adopt the simplest models, namely the crystal field model in the conditions of the low recognition of the input anisotropy parameters of the commensurate UFe_4Al_8 [H8] and the distribution of magnetization in an incommensurate ScFe_4Al_8 [H9]. The last of mentioned papers concerns the magnetization mapping of non-collinear and incommensurate system at zero magnetic field condition. In the case of non-collinear system use of appropriately strong magnetic fields, i.e. 5 T relative to ~ 15 T associated with $\sim 1 \mu_B$ magnetic moment of an iron atom does not change true values of the magnetic moments, but it could reorient the spin directions into the external magnetic field direction, and in this way modify the spontaneous magnetic ordering of the tested system. Such modification of the magnetic ordering would be an extra effect controlling the directional magnetocrystalline anisotropy and thus would support magnetic exchange interactions along certain direction.

Due to the use of a few basic techniques: XRD (X-ray Diffraction), ND (Neutron Diffraction), Laue (registration Lauegrams in transmission geometry), MS (Mössbauer Spectroscopy), MCPMS (Monochromatic Circularly Polarized Mössbauer Source), magnetization measurements of FC (Field Cooling) and ZFC (Zero Field Cooling) scenarios and SEM (Scanning Electron Microscopy) used in basic research in solid state physics in relation to a very specific group of incommensurate structures the intention of the Authors was also the comparison of obtained experimental results relating to research the magnetic properties of MFe_4Al_8 ($M = f$ - elements, Sc) systems in the context of documented properties of the other members of this family. The f -electron elements are divided into two families, namely Lanthanides and Actinides. Lanthanides characterize unfilled $4f$ electron shell and behave normally as the free atoms or ions with a well localized magnetic moment. In contrast

the Actinides with unfilled $5f$ electron shell remain poorly known, particularly their "whimsical" magnetic character. Light Actinides including thorium and uranium possess less localized $5f$ electrons whose energies are close to the energies of $7s$ - electrons and $6d$ -ones. The proximity of the energy bands favors the interactions between the electrons ($5f$) - ($6d$, $7s$). The electronic structure calculation show a variety of the spin-orbital interactions, which result in sophisticated magnetic structures [2^{ii} , 3^{iii} , 4^{iv} , 5^{v}]. On the other hand we are dealing with a similarly complex magnetic ordering of which can only be the result of intra- and inter-atomic spin-spin interactions observed between atoms of Fe and Sc in isostructural intermetallic compounds. The magnetic properties of Actinide largely depend on the distance between the Actinide atoms. The influence of distance Actinide - Actinide on the interaction between $5f$ electrons was analyzed by Hill [6^{vi}]. According to the diagram of temperatures of phase transitions as a function of distance Ac - Ac there is a critical distance U - U approximately 3.5 \AA , below which at low temperatures the Pauli paramagnetism or relatively superconductivity occur while above this value magnetic ordering appears.

2 MODULATED MAGNETIC STRUCTURE OF ScFe_4Al_8 BY X-RAY, NEUTRON POWDER DIFFRACTION AND MÖSSBAUER EFFECT [H1]

In the presented work the results of X-ray and neutron diffraction end Mössbauer spectroscopy measurements carried out on ScFe_4Al_8 sample are discussed. X-ray and neutron diagrams recorded at room temperature showed that the analyzed system crystallizes in the body centered tetragonal structure with space group $I4/mmm$ no. 139. Figure 1 illustrates a typical for these compounds f - j disordering of the order of 4% and of about 6% a - f

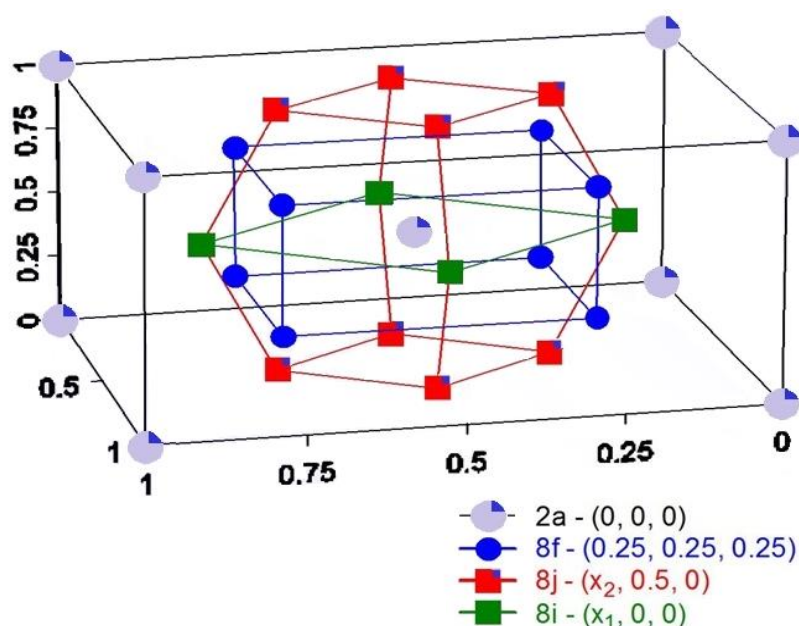


Figure 1. Crystal structure of MFe_4Al_8 system.

disordering not observed in other compounds of this family. Moreover, a traces of unknown extra phase of Fe-Sc origin was observed. The orthorhombic symmetry of an extra phase is visible in the form of several reflections for 2θ above 17° (the left panel of Figure 2). In the temperature range of 8 K-187 K the neutron diagrams had systematically disclosed magnetic satellites around the (110) nuclear reflections. The similar neutron diagrams were collected in the case of Lanthanide compounds REFe_4Al_8 (RE = La, Ce, Tb, Er, Lu) and in the case of a transition metal YFe_4Al_8 [2ⁱⁱ- 4^{iv}]. However, in the family of Actinide compounds the magnetic satellites were collected in the case of ThFe_4Al_8 only (the right panel of Figure 2) [7^{vii}]. It is worth noting that isostructural uranium compound UFe_4Al_8 [8^{viii}, 9^{ix}] is characterized by a commensurate magnetic structure. In the case of magnetic structures of Lanthanides compounds with the magnetic scattering vector $q \neq q_0 = (0, 0, 0)$, i.e. modulated structures were observed both in heavy Lanthanides samples as Tb or Er - clearly magnetic atoms as well as light ones - La, Ce of negligibly low, their own magnetic moment.

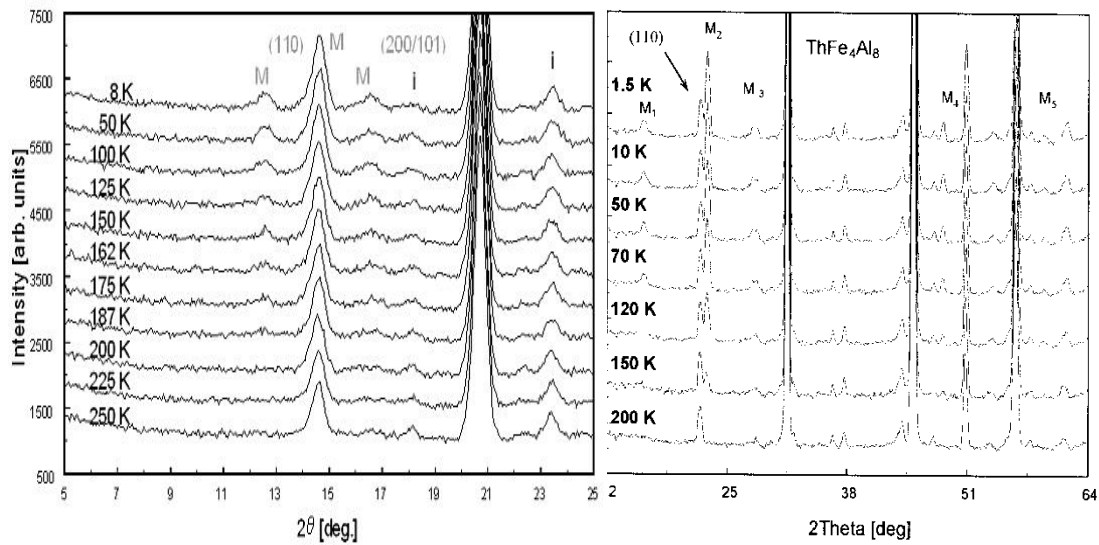


Figure 2. Neutron powder diffraction diagrams versus temperature for ScFe_4Al_8 (left panel) and for ThFe_4Al_8 (right panel) samples. The reflections marked by ‘M’ have pure magnetic origin and ‘i’ indicates an impurity. The indexed diffraction maxima (hkl) belong to the nuclear structure only.

In contrast to the double-modulated ThFe_4Al_8 , with the magnetic scattering vectors: $q_{xy} = (0.279(2), 0.279(2), 0)$ and $q_z = (0, 0, 0.204(2))$ the polycrystalline $\text{Sc}_{0.946}\text{Fe}_{3.934}\text{Al}_8$ sample disclosed $q_{xy} = (0.136(2), 0.136(2), 0)$ modulation which does not change with

temperature up to 175 K. The aluminum atoms stabilize the crystal structure and since have almost zero magnetic moment, do not influence essential magnetic properties of the system. The iron atoms carry magnetic moment of $1.08(12) \mu_B$, while scandium ones are treated as non-participating in the formation of the magnetic structure. The spins of the iron atoms form a flat spiral in the basal ab plane rotating by $49(1)^\circ$ from cell to cell. The angle of rotation, $\frac{\pi}{4}$, perfectly explains the lack of any Zeeman sextets's asymmetry, observed at 12 K, measured by polarized radiation, indicating a strong antiferromagnetic coupling without generating any ferromagnetic component. During measurements Such a ferromagnetic component would be easy to observe by use circularly polarized Mössbauer source. Any asymmetry of amplitudes of lines 1 and 6, and 3 and 4 in Zeeman sextets recorded at the external field of 1 T were not observed. The iron magnetic moment $-1.24(8) \mu_B/\text{atom}$ – was estimated by use coupling constant typical for bcc Fe_α structure assuming that the hyperfine field values $\sim 33T$ of mentioned ferromagnet corresponds to $2.2 \mu_B$ per Fe atom.

However, given the relatively weak intensities and poor collection of satellite reflections Authorees was aware of the incomplete analysis of the extinction rules. For this purpose, the single crystal studies of the scandium compound were undertaken on.

3 MAGNETIC PHASE TRANSITIONS IN $ScFe_4Al_8$ BY POWDER AND SINGLE CRYSTAL NEUTRON DIFFRACTION [H2]

The neutron and Mössbauer results were related to the $Sc_{0.946}Fe_{3.934}Al_8$ powder. In the scandium compound one type of magnetic modulation with rotation angle close to the value of $\frac{\pi}{4}$ was observed. These results did not explain the characteristics of magnetization curves revealing the weak nature ferromagnetic of the system. The small coercive fields observed by use VSM magnetometer, clearly pointed out the ferromagnetic nature of the sample (Figure 3). Neutron measurements allowed determine a phase transition temperature of ~ 220 K. However, due to weak magnetic signals have failed to resolve which of magnetic models (Figure 4) is the most probable one.

The considered magnetic models involved the iron magnetic moments oriented along the directions of high symmetry, i.e. $[100] = [010]$, $[001]$ and $[101]$ and all of them consistently demonstrated low temperature value of the magnetic moment of the iron about $1\mu_B/\text{atom}$. Noteworthy, none of these models would not explain a weak ferromagnetism. Therefore, many efforts have been made to obtain an ordered single crystal having a composition consistent with the nominal composition, which was confirmed during high resolution X-ray and neutron measurements.

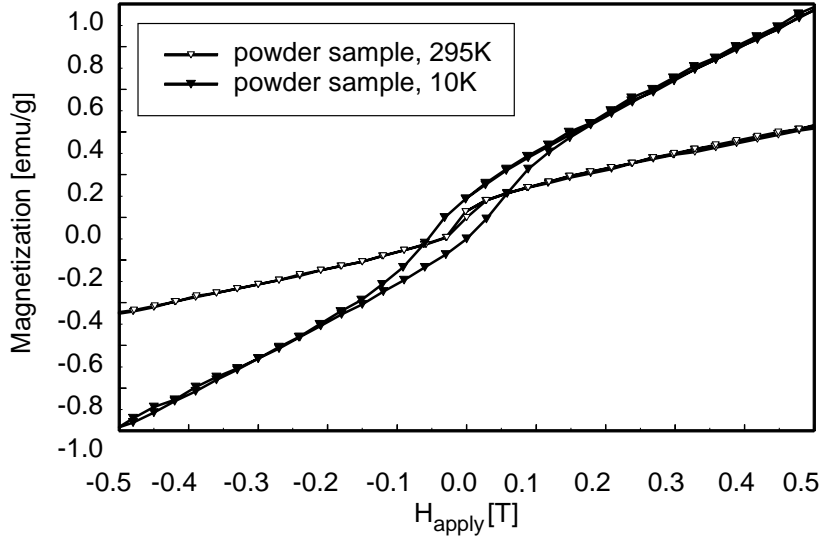


Figure 3. Field dependence of the magnetization at 10 and 295K measured with increasing and decreasing field strength in the range of (-0.5, 0.5) T for polycrystalline sample.

Moreover, according to neutron measurements it turned out that in a system containing scandium atoms the two qualitatively different long-term magnetic modes type of $q_{\perp c} = (\pm q_x, \pm q_x, 0)$ are realized. While the iron atoms still carry a magnetic moment of about $1 \mu_B$. The magnetocrystalline anisotropy, with a negligible magnetic contribution of scandium atoms would have to be supported by a broken symmetry surrounding the iron atoms.

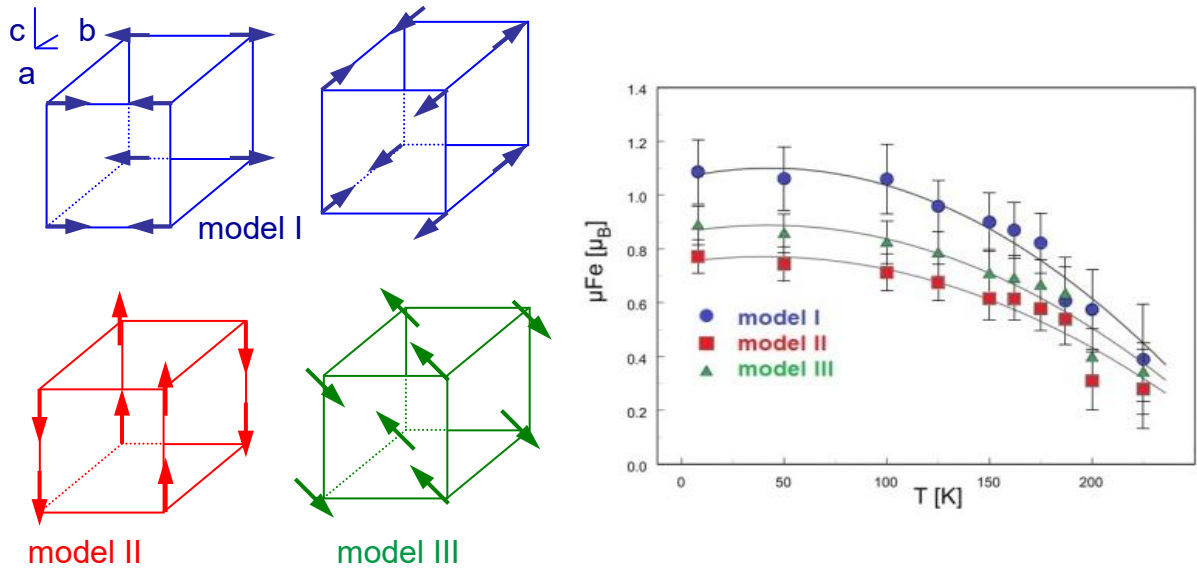


Figure 4. Basic antiferromagnetic distribution of Fe(8f) spins in ScFe_4Al_8 explaining powder diffraction data equally well (left part of the panel) and the temperature behavior of the Fe

magnetic moments obtained for this models. Model I: $G(++-)$ where G_{xx} and G_{yy} are equivalent by symmetry. Model II: $I(++-)$.

Single crystal of ScFe_4Al_8 reveals the presence of a magnetic modulation $\vec{q}_1 = (\pm 0.13, \pm 0.13, 0)$, but much more magnetic reflections associated with modulation $\vec{q}_2 = (\pm 0.18, \pm 0.18, 0)$ were collected. In light of these results the simplest expected magnetic structure seems to be a double cycloid spiral. According to LT neutron measurements the two magnetic modulations are comparatively strong (Figure 5).

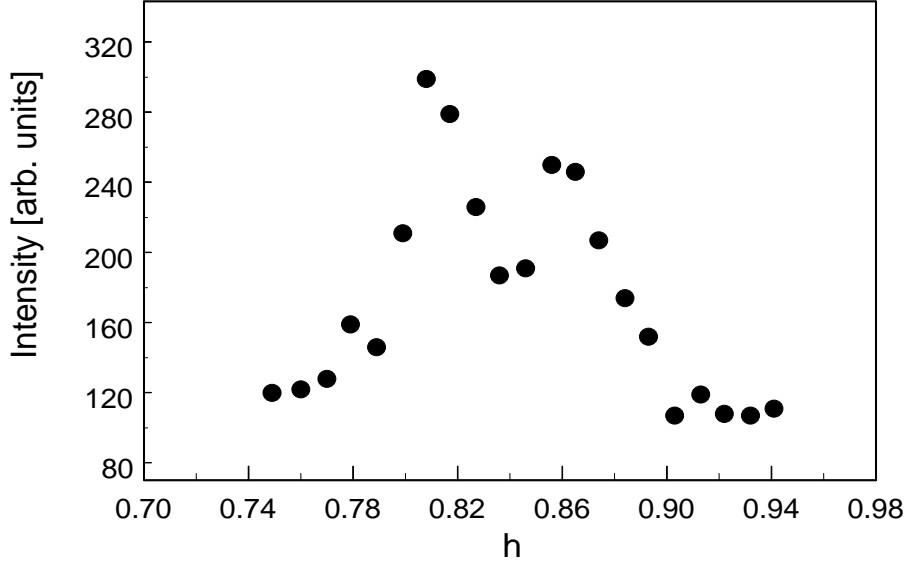


Figure 5. The diffraction pattern collected at temperature $T = 8$ K along the $[110]$ direction near of the reciprocal lattice point (110) . Two independent diffraction maxima are observed at $h = 0.82$ and 0.87 .

The convenient formulas of the structure factors allowed for relatively simple structural analysis of the extinction rules. This analysis led to the conclusion that in the case of a simple type of modulated ferromagnetic material following reflections (hkl) with $h, k = 2n + 1$ and $l = 2n$ for example (110) , (112) are allowed, while (200) , (220) etc. are forbidden. This is exactly the nature of satellite reflections associated with modulation $\vec{q}_1 = (\pm 0.13, \pm 0.13, 0)$. While the observations associated with the modulation $\vec{q}_2 = (\pm 0.18, \pm 0.18, 0)$ indicates a different type of magnetic ordering. For the last one very strong magnetic satellites around the nuclear reflections (hkl) with $h, k, l = 2n$ are observed. Thus, \vec{q}_2 modulation is not implemented by the ferromagnetic system, the easiest option is the modulated spin-canted system in the likeness of UFe_4Al_8 . Summarizing, around the nuclear reflection (110) eight

satellite reflections were collected. Fully consistent observations were found around (112) and (310) nuclear peaks while, around the (hkl) with $h, k, l = 2n$ systematically four reflections associated with the magnetic modulation $\vec{q}_2 = (\pm 0.18, \pm 0.18, 0)$ only were observed (Table 2 of H2 paper).

The magnetism of the system is explicitly complex. Obviously, due to the richer magnetic information obtained by single-crystal research the revision of the earlier collected powder neutron data was taken (Figure 6). The expected spin ordering and different length of the second magnetic scattering vector allowed analyze by simulation the possibility of covering Bragg reflections related to second magnetic modulation. Finally, there are no signals from the expected contribution of modulation \vec{q}_2 . Particularly easy to observe would be the expected intensity of purely magnetic peak $(\bar{1}\bar{1}0) + q_2$, while this reflection is not visible on presented neutron diagram.

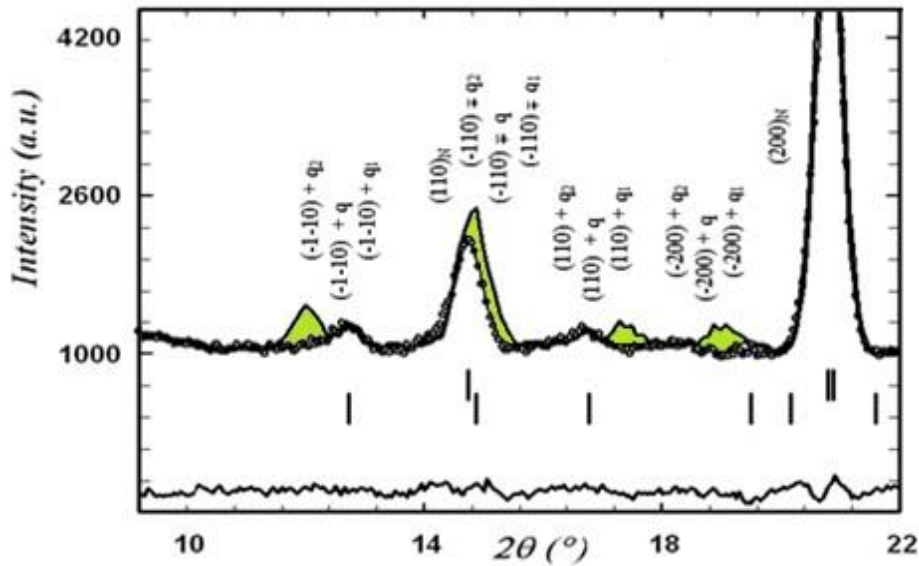


Figure 6. Observed, calculated and difference neutron diagrams of ScFe_4Al_8 powder sample measured at 8 K. The indexing $(hkl) + q_1$ refers to the magnetic satellites present in all powder patterns up to 175 K. The additional solid line overlapped to observed diagrams presents the simulated spectra, where the contribution of both magnetic modulations q_1 and q_2 found in the single crystal measurements were taken into account.

Due to the large number of magnetic satellites of both types, i.e. $(2n + 1, 2n + 1, 2n)$ and $(2n, 2n, 2n)$ associated with the modulation \vec{q}_2 it was also examined the distribution of domain in the ScFe_4Al_8 system (Table 1). The neutron data clearly grouped into two sets

depending on the direction of observation namely going from $\pm[110]$ to $\pm[\bar{1}10]$ one gets reversed sequence of structure factors (see Table 2 of H2 paper) for $(q_2, q_2, 0)$ and $(-q_2, q_2, 0)$ satellites. In other words the magnetic structure rotates by 90° , see also Table 1. This strongly indicates the effect of magnetic domains in the crystal. Summing up, the magnetic structure can be described as almost pure antiferromagnetic double cycloid spiral system. However, from the perspective of the face diagonals, $[110]$ and $[\bar{1}10]$, the pairs of iron atoms form a ferrimagnetic double-flat cycloid spiral structure. Noteworthy, even small ferromagnetic component would transfer magnetic symmetry from double cycloid spiral (DCS) to much more complicated double cone cycloid (DCC) one.

Table 1. Scheme of the magnetic structure associated with the vector $\vec{q}_2 = (\pm 0.18, \pm 0.18, 0)$, shown on the right figure, approximates the geometry conditions of the domain described by parameters set out in column 3 based on single crystal measurements.

| Parameters | $\bar{F}_{(hkl)+(q_2, q_2, 0)}^2$ | $\bar{F}_{(hkl)+(q_2, -q_2, 0)}^2$ |
|------------|-----------------------------------|------------------------------------|
| | $\bar{F}_{(hkl)-(q_2, q_2, 0)}^2$ | $\bar{F}_{(hkl)+(-q_2, q_2, 0)}^2$ |
| μ_{Fe} | $1.23(6)\mu_B$ | $1.19(8)\mu_B$ |
| Φ_1 | $318(9)^\circ$ | $46(9)^\circ$ |
| Φ_2 | $248(6)^\circ$ | $353(9)^\circ$ |

Summing up this part of the study of the single crystal it can be concluded that all of the observed reflections related to the magnetic modulation \vec{q}_2 allowed for a precise description of the magnetic structure and a picture was very similar to that one observed in UFe_4Al_8 . The resultant magnetic moment of the iron atom is consistent with the one obtained from neutron powder measurements ($\sim 1 \mu_B$). Moreover, as a part of the obtained solution, the intensity of reflections satellite confirmed the distribution of domains perpendicular to each other. The phase transition temperature associated with the modulation of \vec{q}_1 perfectly agrees with the previously observed in the powder measurements ~ 220 K.

The phase transition temperatures observed for the single crystal in the temperature range 5 – 250 K indicate a possibility of creating two subsystems of magnetic moments forming different magnetic structures: one antiferromagnetic and the other one described as weak ferromagnetism. Figure 7 illustrates that, these structures clearly exhibit different thermal dynamic: the q_1 modulations exists below 220 K while the modulation with q_2 exists below 130 K.

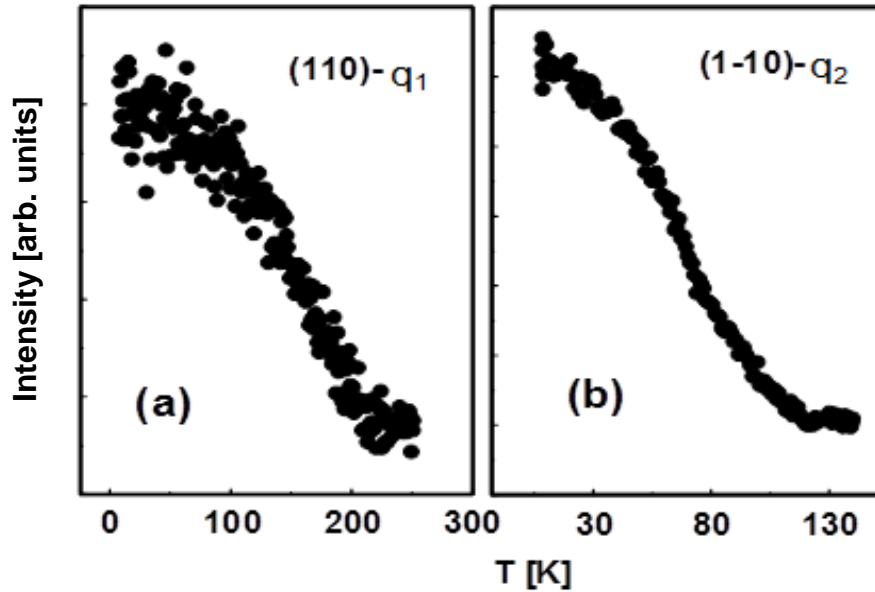


Figure 7. Thermal variation of the integrated neutron intensities of the satellites $(110) - \left(\frac{2}{15}, \frac{2}{15}, 0\right)$ and $(1\bar{1}0) - \left(\frac{9}{50}, \frac{9}{50}, 0\right)$ obtained on ScFe_4Al_8 single crystal are shown in (a) and (b), respectively.

The magnetic structure related to vector \vec{q}_2 (not observed previously) and with a larger period of 50 elementary cells, vanishes much faster, above 120 K already (Figure 7b). These properties indicate the ideal long-range ordering which could be disrupted in the powder samples by scandium deficient and dual kind namely a - f and f - j of structure disorder. According to the kinematic diffraction theory in powder samples the intensity of the reflection is proportional to the square of the number of unit cells contained in a specific volume. In order to see well a modulation vector i.e. the coherent scattering the certain periodicity conditions are required. Analyzing the dimensional effect is noteworthy that \vec{q}_2 modulation is realized in the elementary supercells of volume $(50 \times 50 \times 1)(8.6 \times 8.6 \times 5)\text{\AA}^3 = 2500 \cdot 370 \text{\AA}^3$, while \vec{q}_1 requires much smaller volume of supercells $(15 \times 15 \times 1)(8.6 \times 8.6 \times 5)\text{\AA}^3 = 225 \cdot 370 \text{\AA}^3$. Therefore the coherent scattering in this case occurs about 10 times more effective in the same volume of material, which could explain the lack of \vec{q}_2 vector observations at powder measurements. Even comparing the size of a typical grain, e.g. 10 μm to the length at which magnetic structure described by modulation \vec{q}_2 locks-in it easy to

calculate that $n = \frac{10^{-5}m}{50 \times 8.6 \times 10^{-10}m} = \frac{10000}{430} \approx 23$ such supercells magnetic housed in grain length, so on the surface there are nearly $n^2 \approx 530$. Whereas for the magnetic structure described by modulation \vec{q}_1 there will be an order of magnitude higher, i.e. more than $n^2 \approx 6000$.

In addition to the single crystals neutron measurements the magnetization ones were also recorded. Figure 8 illustrates the temperature characteristics of magnetization collected for the cooled single crystal (Figure 8) in the external field of 0.015 T and without the field. They confirmed anomaly in the phase transition temperature ~ 115 K associated with the modulation of \vec{q}_2 .

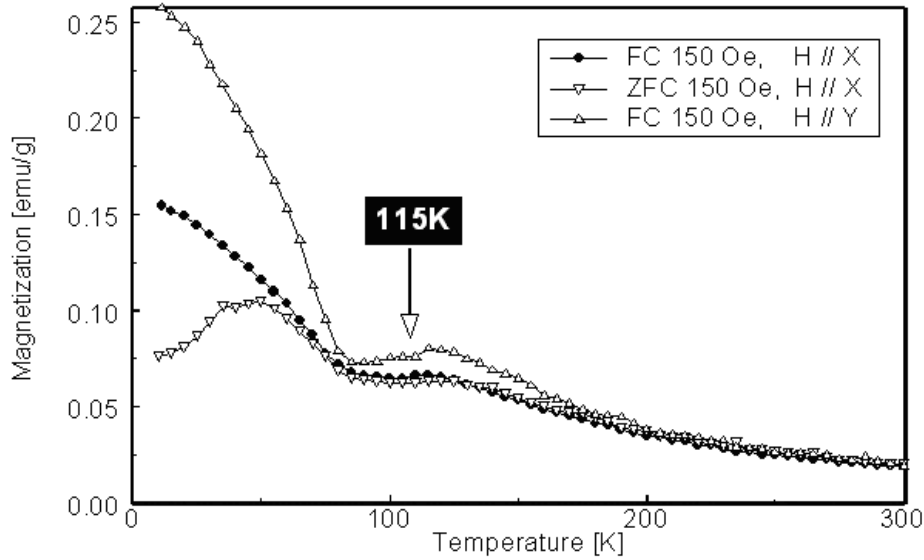


Figure 8. Magnetization curves against temperature, measured in an applied field of 0.015T. The block of the single crystal was cooled in the field (FC) and without the field (ZFC). The X, Y, Z - conventional mutually perpendicular directions of the sample.

4 MAGNETIC PHASE TRANSITIONS IN SCFE_4AL_8 [H3]

The analysis of the magnetism around iron atoms in scandium alloy shows that within the first few coordination zones (of width of about 0.1 \AA) the magnetic atoms are present only in Ist, IIIrd and Vth coordination zones around the selected iron atom position (Figures 9a-f).

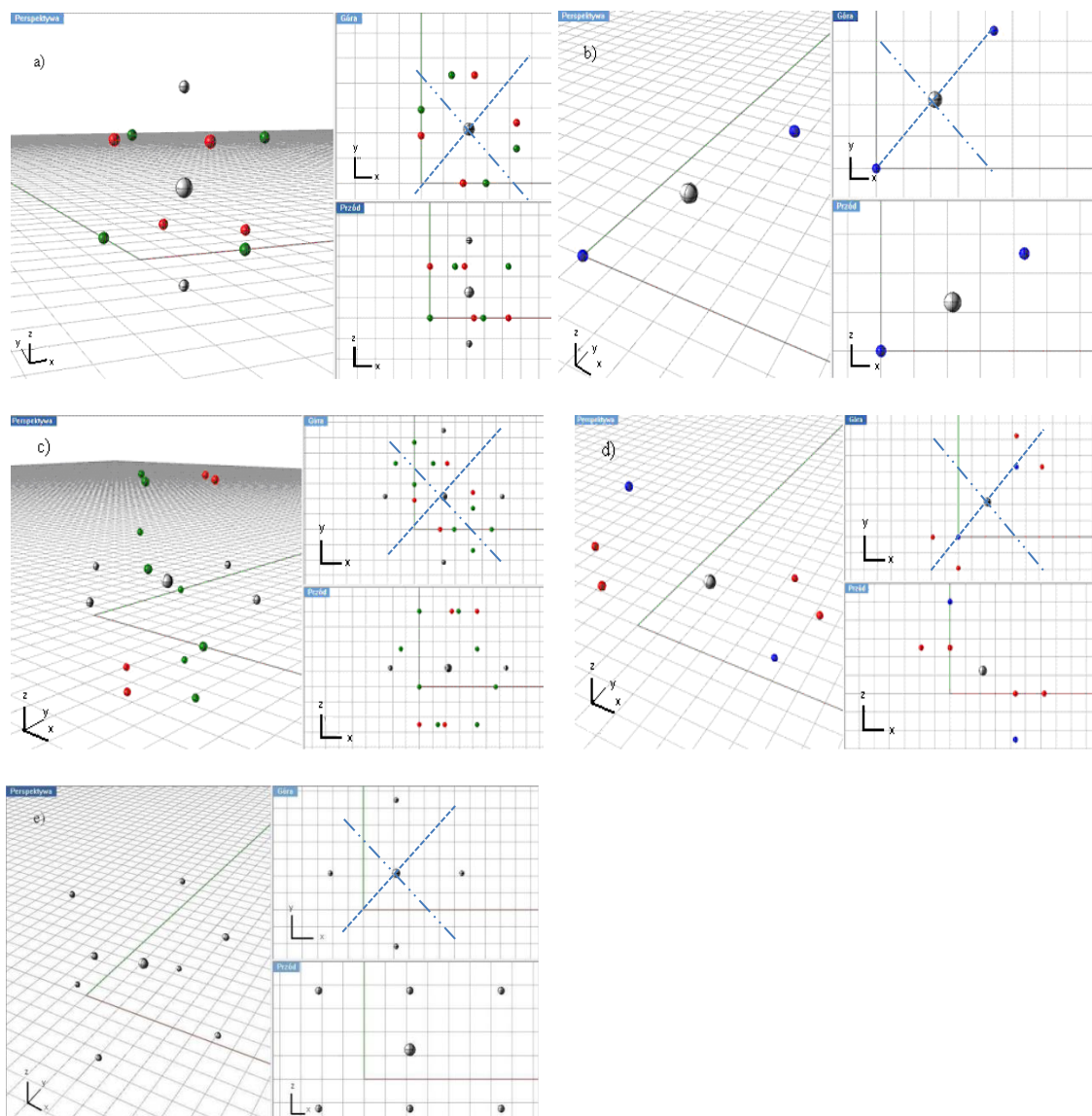


Figure 9. Projections of five coordination zones around the crystallographic position (f) in a plane parallel and perpendicular to the xy basal plane described by symmetry axes along the directions of magnetic modulation propagation in a perfectly ordered MFe_4Al_8 structure of $I4/mmm$ symmetry. Legend: gray positions - $(8f)$ neighbors, blue positions - $(2a)$ neighbors, green positions - $(8j)$ neighbors and the red positions - $(8i)$ neighbors.

Further on it was shown that at a distance not exceeding the shorter lattice parameter the atoms with magnetic moments are far away from each other. The scandium atoms similarly to other weakly magnetic or ‘nonmagnetic’ Actinides occupying II and IV zones can participate in magnetic interactions by superexchange or polarization mechanism, which would facilitate and partly enhance the magnetic modulation along [110] direction (Figure 5b and d – projections on xy plane). No similar effect along the direction of $[\bar{1}10]$ is observed, and therefore the exchange interactions along this direction must be controlled by other rules. It follows from the symmetry conditions that the natural consequence of the presence of the vector form $\vec{q}_i = (q_i, q_i, 0)$ are four satellite reflections: $(110) - \vec{q}_i$, $(1\bar{1}0) - \vec{q}_i$, $(1\bar{1}0) + \vec{q}_i$ and $(110) + \vec{q}_i$. A pair of reflections namely $(1\bar{1}0) \pm \vec{q}_i$ occurs at the same Bragg angle. Indeed, at a temperature of 1.5 K around the first, allowed by symmetry, nuclear reflection (110) three distinct reflections of the magnetic satellites were recorded. Beyond doubt and irrespective of crystalline form, scandium compound retains noncollinear and incommensurate spin structure. It should be noted that the tested sample is doubly modulated and each modulation possess a different temperature of phase transition. According to the results of symmetry analysis, the following conditions of the arrangement of iron magnetic moments were obtained with the help of the computer program MODY [10^x]: the 8 atomic positions are spliced into two independent orbits.

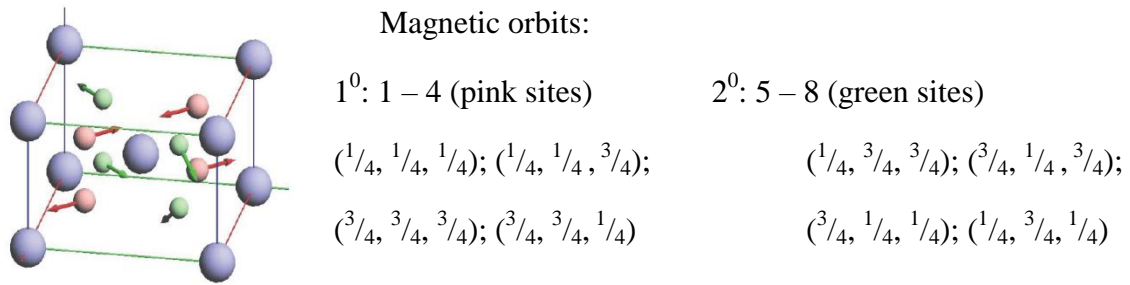


Figure 10. View at "0th" magnetic cell, in which two magnetic orbits resulting from the modulation $q_{xy}=(\pm q_x, \pm q_x, 0)$ were distinguished.

Representations that can be implemented and for some of the Lanthanides compounds [2ⁱⁱ, 3ⁱⁱⁱ] are really observed do not exclude the presence of a magnetic component along the c -axis, which would indicate the conical magnetic structure and contribution of the magnetic scattering into $(2n\ 2n\ 2n)$ nuclear type reflections.

The intensities of the diffraction pattern are the information obtained from the experiment directly:

$$I_{(hkl)} \propto |F_{(hkl)}|^2 \quad \text{wherein in the case of magnetic intensity } |\vec{F}_{(hkl)}|^2 = \vec{F}_{(hkl)} \cdot \vec{F}_{(hkl)}^* \quad (1)$$

The geometric structure factor of commensurate magnetic structure describes the classical equation (2), wherein ξ_j is Halpern vector:

$$\vec{F}_{(hkl)} = 0.27 \cdot \sum_{j=1}^N \vec{\xi}_j \cdot \mu_j \cdot f_{m_j} \cdot \exp\{2\pi i(hx_j + ky_j + lz_j)\} \quad (2)$$

In the case of incommensurate magnetic structure, in which the type of modulation vector was described as $\vec{q} = (\pm q_x, \pm q_x, 0)$ the above expression modifies to form:

$$\vec{F}_{(hkl)\pm\vec{q}} = 0.27 \cdot \sum_{j=1}^N \vec{\xi}_j \cdot \mu_j \cdot f_{m_j} \cdot \exp\{2\pi i((h \pm q_x)x_j + (k \pm q_y)y_j + lz_j)\} \quad (3)$$

The proposed model for in-plane distribution of the Fe magnetic moments at positions (8f):

1-4: $\mu(\cos 2\pi(\Phi_1 + q_i \cdot R_T), \sin 2\pi(\Phi_1 + q_i \cdot R_T), 0)$ and 5-8: $\mu(\cos 2\pi(\Phi_2 + q_i \cdot R_T), \sin 2\pi(\Phi_2 + q_i \cdot R_T), 0)$, where $q_{i=1,2} \Rightarrow q_1 = 0.133$ and $q_2 = 0.18$ up to ~ 120 K, while above this temperature until 230 K $q_{i=1} \Rightarrow q_1 = 0.133$, and R_T is a vector of primitive translation of the relevant system in a real space. The magnetic moments of each orbit are, for simplicity, the same value but different phases. Assuming in-plane distribution of magnetic moments and taking into account Halpern vector magnetic structure factors finally are described by the expression:

$$\vec{F}_{(hkl)\pm\vec{q}} = 0.27 \cdot \sum_{j=1}^8 \left(\begin{array}{l} \cos\Phi_j - \frac{h\pm q_x}{(h\pm q_x)^2 + (k\pm q_y)^2} \{(h \pm q_x)\cos\Phi_j + (k \pm q_y)\sin\Phi_j\} \\ \sin\Phi_j - \frac{k\pm q_y}{(h\pm q_x)^2 + (k\pm q_y)^2} \{(h \pm q_x)\cos\Phi_j + (k \pm q_y)\sin\Phi_j\} \end{array} \right) \cdot \mu_j \cdot f_{m_j} \exp\{2\pi i((h \pm q_x)x_j + (k \pm q_y)y_j + lz_j)\} \quad (4)$$

Let the origin of the system will be connected with the first magnetic position. Then the another ones (x_j, y_j, z_j) take the form: 1 – (0, 0, 0), 2 – (0, 0, 1/2), 3 – (1/2, 1/2, 1/2), 4 – (1/2, 1/2, 0), 5 – (0, 1/2, 1/2), 6 – (1/2, 0, 1/2), 7 – (1/2, 0, 0), 8 – (0, 1/2, 0), and the magnetic structure factor $\vec{F}_{\vec{G}\pm\vec{q}}$ can be described by the formula:

$$\vec{F}_{\vec{G}\pm\vec{q}} \propto \mu \cdot f_{Fe} \cdot \{(1 + e^{i\pi l} + e^{i\pi(h+k+l)} + e^{i\pi(h+k)}) \cdot e^{i\Phi_1} - (e^{i\pi(k+l)} + e^{i\pi(h+l)} + e^{i\pi h} + e^{i\pi k}) \cdot e^{i\Phi_2}\} \quad (5)$$

let $\Phi_2 - \Phi_1 = \delta\Phi$

$$\vec{F}_{\vec{G}\pm\vec{q}} \propto \mu \cdot f_{Fe} \cdot \{(1 + e^{i\pi l})(1 + e^{i\pi(h+k)}) \cdot e^{i\Phi_1} - (1 + e^{i\pi l})(e^{i\pi h} + e^{i\pi k}) \cdot e^{i\Phi_1} \cdot e^{i\delta\Phi}\} \quad (6)$$

Simplifying expression (6) a dependence of the magnetic structural factor sensitive to the phase difference $\delta\Phi$ of the iron magnetic moments belonging to separate magnetic orbits (6a) is obtained:

$$\vec{F}_{\vec{G}_{\pm\vec{q}}} \propto \mu \cdot f_{Fe} \cdot e^{i\Phi_1} \cdot (1 + e^{i\pi l}) \{1 + e^{i\pi(h+k)} - (e^{i\pi h} + e^{i\pi k}) \cdot e^{i\delta\Phi}\} \quad (6a)$$

For example:

$$\vec{F}_{(200\pm\vec{q})} \propto \mu \cdot f_{Fe} \cdot 4 \cdot e^{i\Phi_1} \cdot (1 - e^{i\delta\Phi}) \quad (6b)$$

$$\vec{F}_{(110\pm\vec{q})} \propto \mu \cdot f_{Fe} \cdot 4 \cdot e^{i\Phi_1} \cdot (1 + e^{i\delta\Phi}) \quad (6c)$$

In the domain distribution due to two sets of magnetic intensity depending on the direction of observation the different estimations of coefficient $\delta\Phi$ were obtained: $\delta\Phi_{\pm(q_2, q_2, 0)} = 70(15)^0$ and $\delta\Phi_{\pm(-q_2, q_2, 0)} = 53(18)^0$.

Weakly ferromagnetic nature of system with the transition temperature of about 115 K is associated with modulation \vec{q}_2 . The presence of magnetic domains is a factor masking here system's ferromagnetism. As expected in the case of modulation \vec{q}_1 no satellite reflections were observed around the nuclear $(2n \ 2n \ 2n)$ ones. The model calculations of magnetic structure factors indicates for phase difference in the different magnetic domains about $\pi/2$. However, consequence of this condition was calculated magnetic almost twice smaller than the experimental magnetic moment of the iron atom. In the case of systems with complex magnetism natural move seemed to be measurements using polarized neutrons, however, expected weak magnetic signals discourage prospective operators of channels with a polarized neutron beams to undertake research in this direction.

5 ON THE CRYSTAL AND MAGNETIC BEHAVIOUR OF SCFe₄Al₈ SINGLE CRYSTAL [H4]

Another issue requiring clarification was the reason of and nodal location of iron atoms realizing two qualitatively different and differently quickly vanishing magnetic modes in the ThMn₁₂ structure. In the structural studies X-ray radiation and the thermal neutron beam were used. Obviously, the wavelengths in the range of 0.54 Å - 5.5 Å are able to interact on the level of typical interatomic distances. Is it in Bragg-Brentano geometry, Debye-Scherrer whether Laue geometry, taking into account the position of the interference maxima and their relationship manages to correctly identify the space group. In crystalline systems of primitive symmetry are not observed systematic extinctions, while in systems with higher symmetries extinction rules give a zero intensities of some of the diffraction peaks. It is similarly, in the case of magnetic structures, typically as a result of more complex than the ferromagnetic spin ordering the number of extinctions rules grows.

The crystals of orthogonal structure with incommensurate magnetic order are a separate class of systems. The diffraction pattern of such incommensurate crystals often characterized by a clear, sharp and well separated Bragg reflections, which cannot be described by three integers indices (hkl) within a given space group. The registered diffraction pattern shows the presence of two groups of reflections. The first group, which includes intensive basic reflections, allows to determine unit cell stretched on $\vec{a}^*, \vec{b}^*, \vec{c}^*$ vectors. The second group contains usually weaker satellite peaks, the description of which requires additional vectors. A complete description of full diffraction diagram by Miller's indexes requires the introduction of additional vectors, and thus the overall \vec{K} vector takes the form:

$$\vec{K}_{hklm} = h\vec{a}^* + k\vec{b}^* + l\vec{c}^* + m\vec{q} \quad (7)$$

while the vector \vec{q} is described as follows:

$$\vec{q} = \alpha\vec{a}^* + \beta\vec{b}^* + \gamma\vec{c}^* \quad (8)$$

Each Bragg reflection has been described by ($hklm$) indexes, where the first three indexes are based on the basal vectors while the last index is related to the q modulation vector. Depending on the values of coefficients α, β, γ , defined as the ratio of the corresponding components of the modulation vector of primitive reciprocal lattice vectors to the base structure, can be divided into two main classes of modulated structures. If the values of these coefficients are rational numbers - modulation is defined as the commensurate (C). C -type modulation can always be expressed in notation (hkl) relating to three-dimensional space. While the crystallographic description of the structures incommensurate (IC) with irrational coefficients α, β, γ requires the superspace. In a typical crystal subnet \bar{x}_j described by the coordinates (x, y, z) can be in the general form written as:

$$\bar{x}_j = R_T + x_j^0 \quad (9)$$

where R_T refers to a primitive translation of the proper symmetry of the crystal while x_j^0 defines the position of the j -th atom in the unit cell. In the incommensurately modulated crystals generated positions are presented as:

$$x_j = \bar{x}_j + u_j(\bar{x}_4) \quad (10)$$

Superspace is a higher dimensional space. The physical three-dimensional space is the supreme terms of extra dimensions, because normally incommensurate crystal is correlated with $(3 + 1)$ - dimensional space. Superspace can describe all the periodicity of the structure including that one associated with modulation. The function $u_j(\bar{x}_4)$ depends on the superspace of coordinate x_4 and its periodicity with respect to translation along a fourth axis. According to the incommensurability of the modulated structure $u_j(\bar{x}_4)$ term added to the

undisturbed position of the atom is different in each adjacent unit cell thereby destroying the three-dimensional translational symmetry of the crystal. Depending on the type of modulation structural function $u_j(\bar{x}_4)$ takes a different form. However, the modulation function is usually developed in a Fourier series:

$$u(\bar{x}_4) = \sum_{n=1}^{\infty} A_n \sin(2\pi n \bar{x}_4) + B_n \cos(2\pi n \bar{x}_4) \quad (11)$$

where for the complete characterization of the modulation the estimation of the amplitudes A_n, B_n is required. The step n of expansion of the Fourier series depends on the experimental data, and is correlated with the index m (7). Overall $x_j(\bar{x}_j, \bar{x}_4)$ atomic position depends on the pair of parameters, the first of which is associated with the basic structure (e.g. outer space), and the second relates to a dimension additional superspace (e.g. inner space). Superspace enables the description of a modulated crystal in group theory: full symmetry of the system is expressed by groups of superspace. The symbol of the superspace group consists of i) the space group of the basic structure, ii) components of the vector q allowed by symmetry and iii) internal translational coordinates along the fourth extra dimension which correspond to all symmetry operators of space group. In order to describe the relationship between atoms in the proposed scheme let example would be to analyze the inversion performance as the superspace operation:

$$(-1|000,0): -x_1 - x_2 - x_3 - x_4 + 1 \quad (12)$$

$$atom\ 1: (x\ y\ z) \rightarrow (-1|000) \rightarrow atom\ 2: (-x - y - z) \quad (13)$$

The phase shifts of any modulation along x_4 not change the energy system. On the other hand superspace translational symmetry, i.e. combination of the lattice translation in real space with a phase shift (the inner space operation of the translational lattice) is described as:

$$\{E|R_T, -q \cdot R_T\} \quad (14)$$

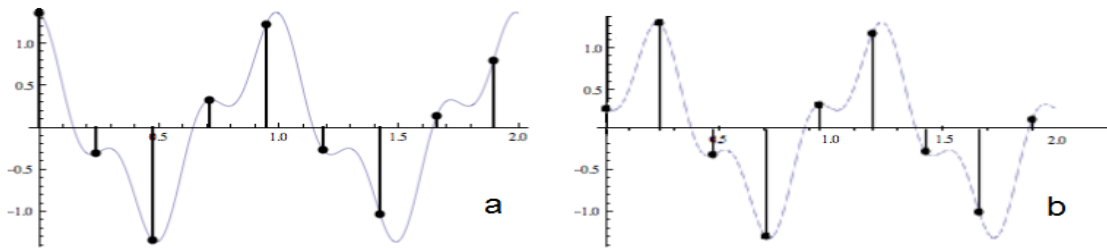


Figure 11. Representation of modulation in the case of lost translational symmetry in real space (a): $\{E|R_T, 0\}$, representation of translation of phase shift (b): $\{E|0, -q \cdot R_T\}$.

The proper notation of space groups is essential during structure refinements. Unfortunately the notation of superspace groups which allows to uniquely describe the modulated nuclear structure, where we deal with shifts of atoms, is not so simple and clear in the description of magnetic structures (Table 2). The magnetic properties of crystals are determined by their magnetic symmetry: a space group (if they are commensurable) or a superspace group (if they are incommensurable).

In making a description of the superspace magnetic groups in the scheme compatible with the presented above for the magnetic moments of atoms 1 and 2 (equation 12 - 13), the following relation is fulfilled: $M_1(x_4) = M_2(-x_4)$ therefore:

$$M_{1_{\sin n}} = -M_{2_{\sin n}}, M_{1_{\cos n}} = M_{2_{\cos n}} \quad (15)$$

If they are identical atoms, then $M_1(x_4) = M_1(-x_4)$ and in further analysis the collinear structure is obtained where all modulations are in phase $\alpha = x, y, z$:

$$M_{1_\alpha}(x_4) = M_{1_{\alpha 0}} + \sum_n M_{1_{\alpha, \cos n}} \cos(2\pi n x_4) \quad (16)$$

If the structure is not collinear for the j -th atom in the P -th unit cell expression (16) takes the form:

$$M_{P_j}(x_4) = M_{j_0} + \sum_{n=1} [M_{j_{\sin n}} \sin(2\pi n x_4) + M_{j_{\cos n}} \cos(2\pi n x_4)] \quad (17)$$

$$M_{P_j} = M_j (x_4 = q \cdot (P + r_j)) \quad (18)$$

An analysis and interpretation of diffraction data for complex modulated structures can be easily performed by use of the commercial programs like *FullProf* [11^{xi}] and *Jana 2006* [12^{xiii}], but it is worth noting the differences in the formalism of recording of spin modulation. Formulas presented above (17-18) applied in *Jana 2006* package were used frequently to analyze the single crystal data, while powder data were carried out based on the software *FullProf* package. It is therefore appropriate to present the same functions used in the *FullProf* that here are as follows:

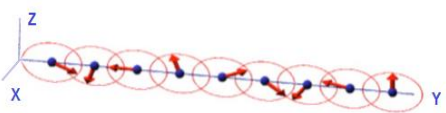
$$M_{P_j}(x_4) = M_{j_0} + \sum_K [S_{K_j} \exp(-i2\pi K \cdot P) + S_{K_j}^* \exp(i2\pi K \cdot P)] \quad (17a)$$

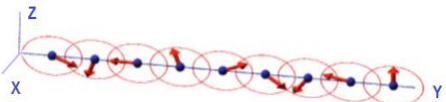
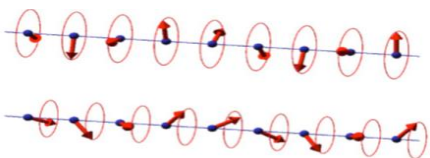
$$S_{K_j} e^{i2\pi K \cdot r_j} = M_{j_{\cos 1}} + iM_{j_{\sin 1}} \quad (18a)$$

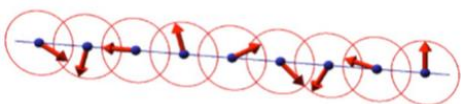
In the case of modulated structures big hurdle is the ambiguity of the above mentioned description of magnetic ordering on superspace groups level. To facilitate potential readers orientation in the following presented table a brief introduction for symmetry aspects of an incommensurability seemed Authors to be necessary. Reaching to database magnetic

structures of *Bilbao Crystallographic Server* [13^{xiii}] one can find irreducible representations, which, according to the group theory can be implemented by the system.

Table 2. Magnetic symmetry of body centred tetragonal (*bct*) system with one magnetic sublattice type of (*8f*) Fe and with two magnetic sublattices type of: (*8f*) and Fe (*2a*) Sc.

| | | | |
|--|--------------------|-----------------------------------|----------------------------------|
| 139.531 $I4/mmm$ [139.1.1179]  | (8f) $\dots 2/m$ | $(1/4, 1/4, 1/4 m_x, -m_x, 0)$ | $(1/4, 3/4, 3/4 m_x, m_x, 0)$ |
| | | $(3/4, 1/4, 3/4 -m_x, -m_x, 0)$ | $(3/4, 3/4, 1/4 -m_x, m_x, 0)$ |
| | (2a) $4/mmm$ | $(0, 0, 0 0, 0, 0)$ | |
| 139.532 $I4/mmm1'$ [139.2.1180] Non-magnetic representation | (8f) $\dots 2/m1'$ | $(1/4, 1/4, 1/4 0, 0, 0)$ | $(1/4, 3/4, 3/4 0, 0, 0)$ |
| | | $(3/4, 1/4, 3/4 0, 0, 0)$ | $(3/4, 3/4, 1/4 0, 0, 0)$ |
| | (2a) $4/mmm1'$ | $(0, 0, 0 0, 0, 0)$ | |
| 139.533 $I4/m'mm$ [139.3.1181] Non-magnetic representation | (8f) $\dots 2/m$ | $(1/4, 1/4, 1/4 0, 0, 0)$ | $(1/4, 3/4, 3/4 0, 0, 0)$ |
| | | $(3/4, 1/4, 3/4 0, 0, 0)$ | $(3/4, 3/4, 1/4 0, 0, 0)$ |
| | (2a) $4/m'mm$ | $(0, 0, 0 0, 0, 0)$ | |
| 139.534 $I4'/mm'm$ [139.4.1182] | (8f) $\dots 2/m$ | $(1/4, 1/4, 1/4 m_x, -$ | $(1/4, 3/4, 3/4 $ |

| | | | |
|--|-----------------|--|--|
|  | | $m_x, 0$ | $-m_x, -m_x, 0$ |
| | | $(3/4, 1/4, 3/4 $ $m_x, m_x, 0)$ | $(3/4, 3/4, 1/4 $ $-m_x, m_x, 0)$ |
| | (2a) $4'/mm'm$ | $(0, 0, 0 0, 0, 0)$ | |
| 139.535 $I4'/mmm'$ [139.5.1183]  | (8f)..2'/m' | $(1/4, 1/4, 1/4 $ $m_x, m_x, m_z)$ | $(1/4, 3/4, 3/4 $ $m_x, -m_x, -m_z)$ |
| | | $(3/4, 1/4, 3/4 $ $-m_x, m_x, -m_z)$ | $(3/4, 3/4, 1/4 $ $-m_x, -m_x, m_z)$ |
| | (2a) $4'/mmm'$ | $(0, 0, 0 0, 0, 0)$ | |
| 139.536 $I4'/m'm'm$ [139.6.1184] Non-magnetic representation | (8f)..2'/m | $(1/4, 1/4, 1/4 $ $0, 0, 0)$ | $(1/4, 3/4, 3/4 $ $0, 0, 0)$ |
| | | $(3/4, 1/4, 3/4 $ $0, 0, 0)$ | $(3/4, 3/4, 1/4 $ $0, 0, 0)$ |
| | (2a) $4'/m'm'm$ | $(0, 0, 0 0, 0, 0)$ | |
| 139.537 $I4/mm'm'$ [139.7.1185]  | (8f)..2'/m | $(1/4, 1/4, 1/4 $ $m_x, m_x, m_z)$ | $(1/4, 3/4, 3/4 $ $-m_x, m_x, m_z)$ |
| | | $(3/4, 1/4, 3/4 $ $m_x, -m_x, m_z)$ | $(3/4, 3/4, 1/4 $ $-m_x, -m_x, m_z)$ |
| | (2a) $4/mm'm'$ | $(0, 0, 0 0, 0, m_z)$ | |
| 139.538 $I4'/m'mm'$ [139.8.1186] Non-magnetic representation | (8f)..2'/m | $(1/4, 1/4, 1/4 $ $0, 0, 0)$ | $(1/4, 3/4, 3/4 $ $0, 0, 0)$ |

| | | | |
|---|-----------------|--------------------------------|--------------------------------|
| | | $(3/4, 1/4, 3/4 0, 0, 0)$ | $(3/4, 3/4, 1/4 0, 0, 0)$ |
| | (2a) $4'/m'mm'$ | $(0, 0, 0 0, 0, 0)$ | |
| 139.539 $I4/m'm'm'$ [139.9.1187] Non-magnetic representation | (8f)..2/m' | $(1/4, 1/4, 1/4 0, 0, 0)$ | $(1/4, 3/4, 3/4 0, 0, 0)$ |
| | | $(3/4, 1/4, 3/4 0, 0, 0)$ | $(3/4, 3/4, 1/4 0, 0, 0)$ |
| | (2a) $4/m'm'm'$ | $(0, 0, 0 0, 0, 0)$ | |
| 139.540 Ic_4/mmm [P4/mmm:123.12.1010]  | (16i)..2mm | $(1/4, 1/4, z m_x, m_x, 0)$ | $(1/4, 3/4, z -m_x, m_x, 0)$ |
| | | $(3/4, 1/4, z m_x, -m_x, 0)$ | $(3/4, 3/4, z m_x, m_x, 0)$ |
| | (4a) $4/mmm$ | $(0, 0, 0 0, 0, 0)$ | |

In the case of magnetic superspace of lower symmetry in the given tetragonal system a variety of modulated structures such as: proper helical, helical transverse conical structure, cycloid or elliptical cycloid can be implemented. Regardless of the method, which is used to determine the magnetic structure, whether derived from the group theory or the extinctions rules based on experimental data, the most reliable solution brings usually combined analysis of both of them. The papers [H6, H7, H8] are devoted to issues of magnetic ordering in single or two different sublattices of MFe_4Al_8 systems.

During the studies the lowering crystal symmetry of the system was considered. However, the lower than expected crystal symmetry not expressly modifying extinctions rules requires specific multiple of the structure ($a \times a \times c$) - such was the idea of present paper. The reason for the lower symmetry of crystal may be escaping experimental sensitivity the disordering type (2a) - (8f). Such effect would increasing with the scandium concentration in the system. For this purpose the neutron experiment with a white beam was carried out.

However, even more efficient geometry instrument Vivaldi (ILL) (Figure 12) using a non-monochromatic beam could not answer conclusively, and presents further doubts regarding the same symmetry of the crystal approving of the description at the same high credibility over 70% of registered spots in the unit cell ($2a \times a \times 2c$) or ($2a \times 2a \times 2c$) (Figure 13).

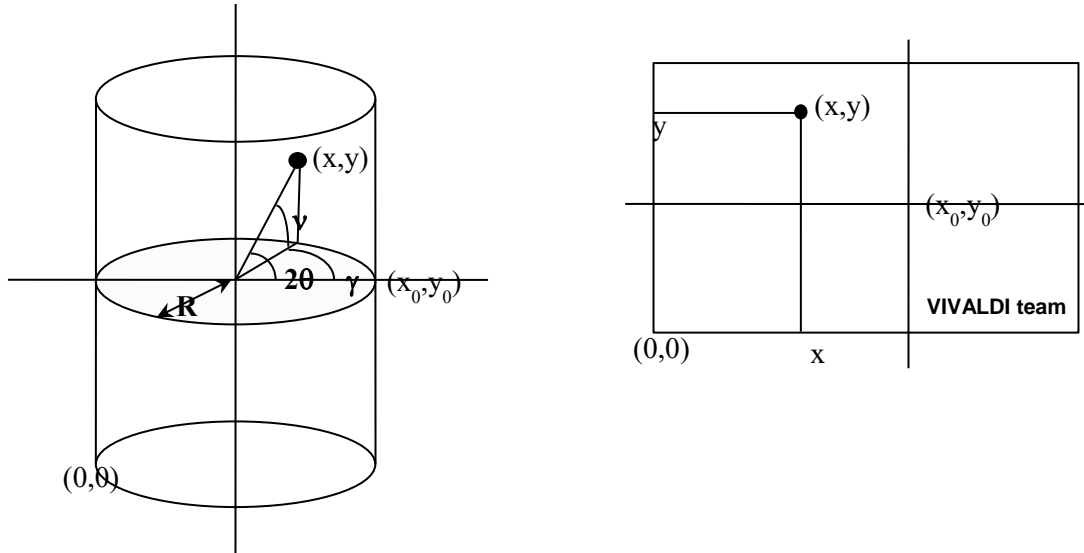


Figure 12. The geometry of the spectrometer Vivaldi (ILL, Grenoble) with defined angles: $\gamma = (x-x_0)p/R$, $\nu = \text{atan}[(y-y_0)p/R]$, $2\theta = \text{acos}[\cos(\gamma)\cos(\nu)]$, where (x,y) is the spot position on the detector (the origin in the lower left corner), p is the pixel size, R - radius of the detector, and (x_0,y_0) is the position of the beam reaching the detector.

As it turned out, only some of the experimentally observed spots fulfill the conditions of the appropriate symmetry. Particularly, the spots localized at the Laue photograph (in red rings), which are not indexed within body centered cell ($a \times a \times c$) require larger unit cell dimensions. Noteworthy, all of the extra peaks have the same shape as those indexed, which means that they are coming from the same part of the crystal, which allow to discard a possible polycrystalline origin. The observed vanishing of the spots above a temperature of 100 K leaves no doubt that the satellites are related to the modulation previously described as \vec{q}_2 . However, the results obtained by means of a Laue technique cannot exclude the participation of the modulation type \vec{q}_1 . Just because of other extinctions rules, magnetic satellites type \vec{q}_1 occur only around the reflection type $(2n + 1, 2n + 1, 2n)$ and not around $(2n, 2n, 2n)$ like for example $(\bar{2}00)$. A folding of the unit cell, keeping its tetragonal body-centered character, but with a doubling of the three cell parameters ($2a \times 2a \times 2c$) allowed to completely simulate of the experimental diffraction patterns. Unfortunately, there is also another unit-cell and symmetry, which can describe Laue's data equally well, namely an orthorhombic primitive unit cell with the dimensions: ($2a \times a \times 2c$). The neutron experiment carried out on VIVALDI turned out to be inconclusive with regard to the exact determination of the general crystal structure.

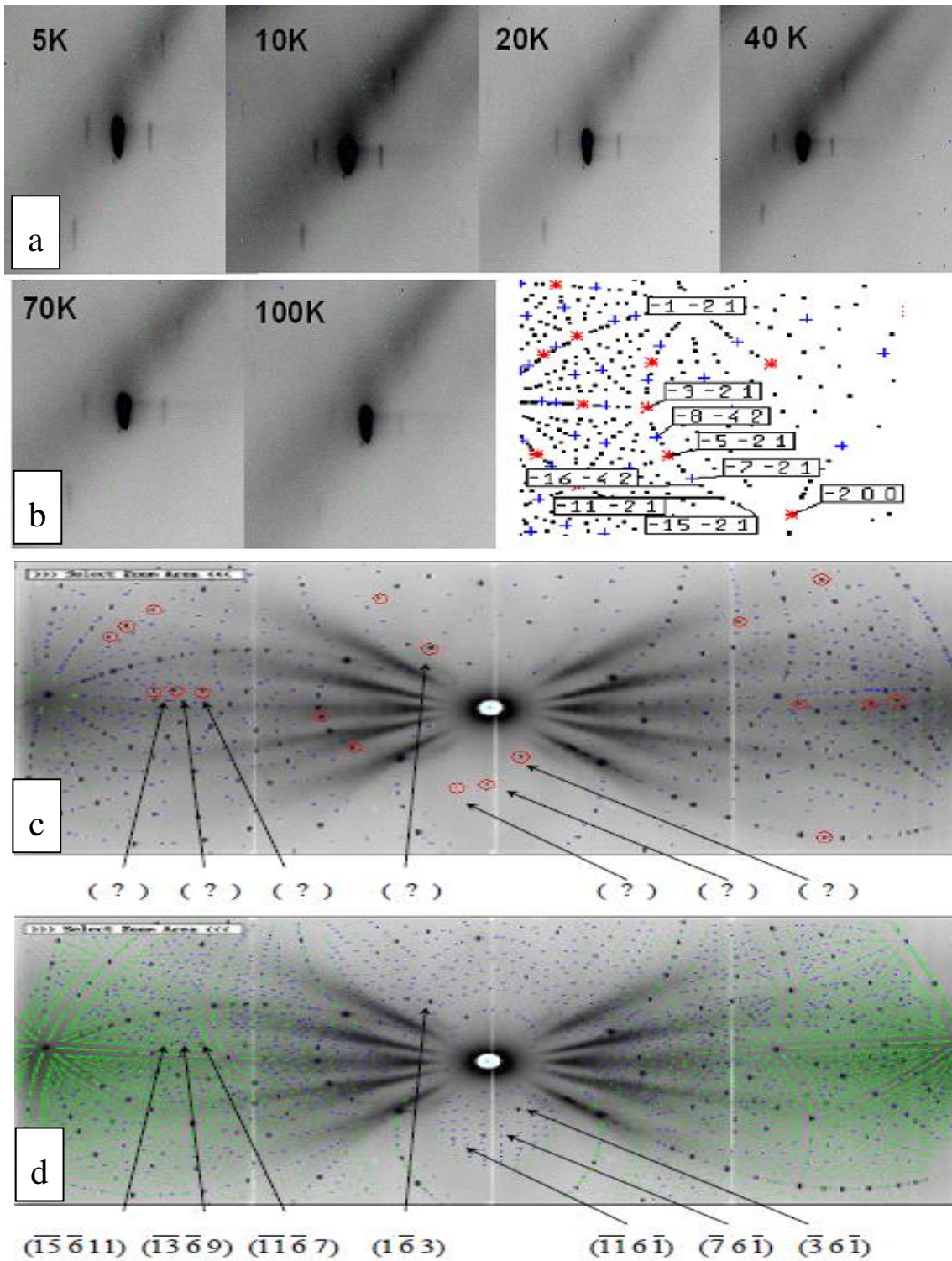


Figure 13. Laueograms registered on Vivaldi spectrometer (upper two rows - a, b) disclose magnetic reflections which are associated with nuclear reflections. The satellites around the reflexes $(\bar{2}00)$ are presented. Laue photographs (the two bottom rows - c, d) illustrate the

experimental data against the base (third projection: $a=b=8.63 \text{ \AA}$ and $c=4.96 \text{ \AA}$) and an 8-fold increased and the unit cell (the fourth projection: $a=b=17.26 \text{ \AA}$, $c=9.92 \text{ \AA}$). The black spots correspond to the experimental ones. The blue points correspond to the primary reflections as described in I symmetry group, while the green points - P symmetry group.

Thanks to a Laue hard X-ray test, using an energy (100 – 400 keV dispersive technique), two intense Bragg reflections were measured at low diffraction angles (Figure 14). They correspond to d -spacing of 4.3 and 2.7 \AA and could be interpreted as respectively the (200) and (310) reflections. However, in both cases, two weak but significant additional reflections were observed at low energy. They correspond to longer d -spacing, forbidden with the I symmetry: ($a \times a \times c$) of unit cell, but which can be easily explained by a cell doubling along both a and b directions. Because of the equatorial geometry of the diffraction experiment, this technique cannot afford information about the c direction. It is noteworthy that none of the analyzed types of doubling due to the spatially centering position do not gives compliance of intensities predicted under the maximum isomorphic subgroups, i.e. cell ($a \times a \times 3c$) or ($3a \times 3a \times c$), which alone do not entail changes to the rules of extinctions. The observed intensity of extra reflections are extremely small in relation to the basic, hence the need to use a logarithmic scale (Figure 14). The left reflection (200) supports the 1 dimension doubling of the unit cell, whereas the presence of the first harmonic of (310) scattering amplitude indicates that the doubling of the unit cell is at least two-dimensional and relates to the base plane xy .

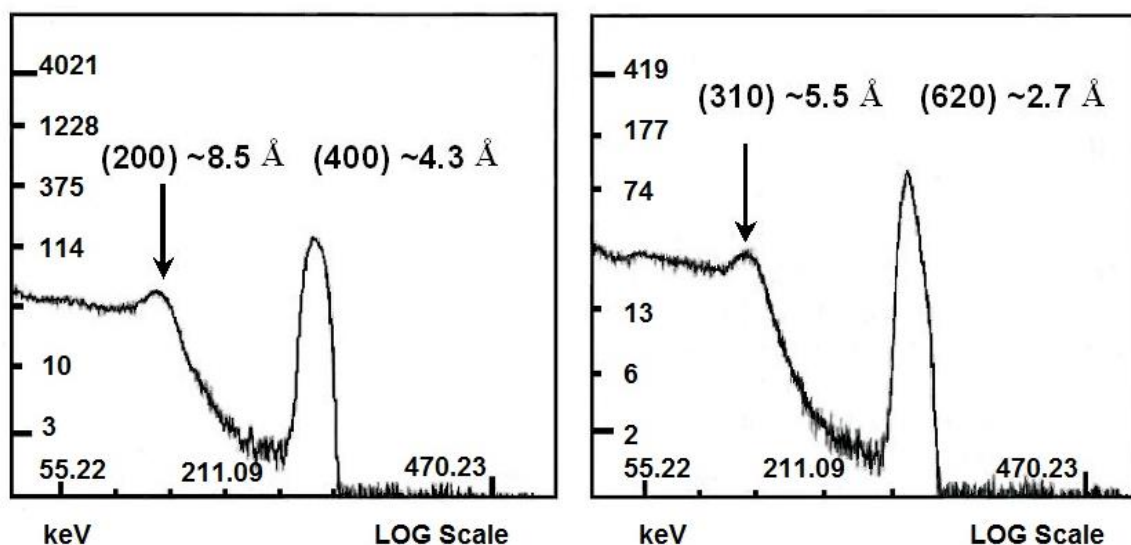


Figure 14. The intensities (shown in logarithmic scale) vs. energy show two Bragg reflections and their harmonics. Presence of (310) reflection (right panel) indicates that the cell parameters' doubling takes place at least in the basal plane.

Regardless of the final solution of symmetry, no evidence of the non-zero z-component of the magnetic moments for both magnetic modulation vectors was found. Nevertheless, the experiment shows that the number of possible models of the magnetic structure has increased and that the magnetic structure de facto should not be treated as a double ‘flat’ cycloid spiral (DCS).

6 STRUCTURAL AND MAGNETIC PROPERTIES OF $\text{Sc}_{1.1}\text{Fe}_{3.9}\text{Al}_8$ [H5]

The source of confusing observation may be so far neglected the influence of scandium and the disordering of type (2a) - (8f), such effect becomes important in systems with excess of scandium concentration.

As a result, it made a series of alloys with a slightly modified proportions of the components which would modify the type of sample magnetism. In a series $\text{Sc}_{1+x}\text{Fe}_{4-x}\text{Al}_8$ the promising system with a trace content of $\text{Fe}_4\text{Al}_{13}$ phase was the system with $x = 0.1$. SEM, XRD and ND studies confirmed excess concentration of Sc, which positioned itself as expected in the sublattice (8f). The magnetic order, type of a double spiral with a slightly smaller modulation vector $\vec{q} = (\pm 0.131(2), \pm 0.131(2), 0)$ with respect to that one found previously at stoichiometric scandium compound and the resultant iron magnetic moment canted by an angle $\alpha \cong \frac{\pi}{12}$ relative to the [110] direction was obtained.

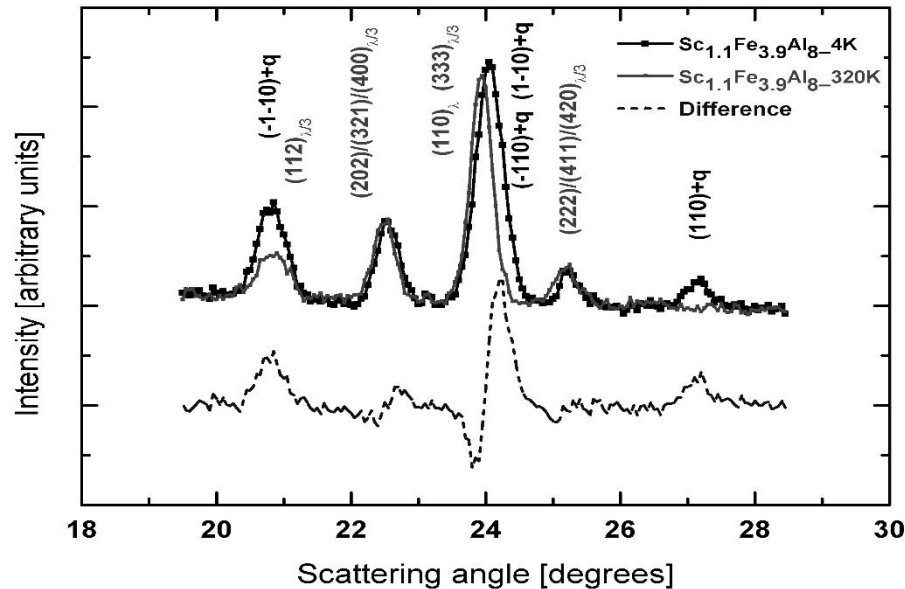


Figure 15. Part of neutron diagrams of $\text{Sc}_{1.1}\text{Fe}_{3.9}\text{Al}_8$ measured at 4 K and the paramagnetic state at 320 K. The difference diagram illustrates scattering amplitudes of purely magnetic origin. The indexing $(hkl) + \vec{q}$ where $\vec{q} = (\pm 0.131(2), \pm 0.131(2), 0)$ refers to the magnetic satellites present up to Néel temperature.

The double spiral system discloses a dominant antiferromagnetic coupling of Fe - Fe in the base plane of the tetragonal cells. The total magnetic moment of iron at easy ab -plane must be $0.87(4) \mu_B \text{ atom}^{-1}$ at 4 K. Because of high statistics achieved, the peak to background ratio observed for the satellites is good enough, and makes the results unambiguous. The spiral arrangement of the magnetic moments applied to the noncollinearity which becomes a constant component of below 120 K, while the canting angle increases from zero to $\frac{\pi}{6}$ at 4 K. Above the temperature close to 120 K the magnetic ordering of the $\text{Sc}_{1.1}\text{Fe}_{3.9}\text{Al}_8$ alloy, consistent with magnetic space group $I4'/mm'm$ (No. 1183), turns into simple incommensurate antiferromagnet which disappears above 230 K. From the classification scheme for magnetic structures based on superspace magnetic groups (Table 2) one can infer, that explanation of the satellites requires considerations of the simplest magnetic space groups, namely $I4'/mm'm$ (No. 1182: $Fmmm$), $I4'/mmm'$ (No. 1183: $Immm$) and $I4/m'm'$ (No. 1185: $I4/m$). These groups lead to the magnetic moments with the following components: $(\mu_x, \mu_y, 0)$, (μ_x, μ_y, μ_z) and $(0, 0, \mu_z)$, respectively. The experimental data presented in this paper support the first possibility.

Finally, the presence of ferromagnetic component coincide with irreversibility observed in magnetization processes (coercivity field). In the temperature range, up to about 230 K, the magnetic structure is double cycloid with propagation wave vector $\vec{q} = (q_\perp, q_\perp, 0)$ and $q_\perp = 0.131(2)$ for temperatures between 0 and ~ 160 K. The magnetic moment of iron is of the order of $0.9 \mu_B$ at 4 K, which corresponds very well to the magnetic hyperfine field $11.2(1)$ T shown by the sextet measured at 16 K. The iron magnetic moments form incommensurate double cycloid structure with the phase shift equal to $150(7)^\circ$ at 4 K. The shift decreases with temperature increase and at ~ 120 K achieves limiting value $\Delta\phi = \pi - 2\alpha + \pi q \Rightarrow \pi(1 + q)$. Observed thermal expansion, particularly negligible expansion at low temperatures, can be explained by anharmonic effects [14^{xiv}, 15^{xv}] with Grüneisen parameter about 2.2. Presence of two magnetic transition temperatures, looks very similar to the situation found in the single crystal of ScFe_4Al_8 [H2, H3 and H4] where two modulation vectors, each disappearing in different temperature, were discovered. A clear difference of results obtained from the single crystal and powder data indicates perhaps a significant influence on the formation of internal stress modulation. A separate issue are the magnetic interactions responsible for the complex spin structure.

To quote my patient mentor Professor Ludwik Dobrzyński: "There is no non-magnetic materials, are the only ones that do not reveal the long-range magnetic order." In the simplest terms, the order of magnetic moments depends on the media type, i.e. the unpaired spins occupied p -type atomic orbitals, and / or f - electron. As part of a carefully studied and presented here tetragonal structures of the ThMn_{12} family, potential partner magnetic interactions with the iron is scandium, which in terms of the magnetic susceptibility is classified as paramagnetic element. As a result of the thermal vibration Sc is characterized by a zero magnetization. In the external magnetic field degree of order of the ferromagnetic phase is small and manifests as the observed finite magnetization. The magnetization causes the appearance of a finite exchange field. This introduction aims to highlight that although scandium in itself is not a carrier of localized magnetic moment, it can significantly modify the exchange interactions of intermetallic compounds. Iron, which is an essential component of all analyzed compounds is ferromagnetic, but depending on local symmetry and type of neighbors it realizes various order types within own sublattice. As a ferromagnet iron characterized by a spontaneous magnetic moment. The so-called exchange field i.e. Weiss field is treated as a magnetic one of induction B . In the mean-field approximation, it is assumed that the field of induction B proportional to the magnetization, $B = \lambda M$, where λ is a temperature independent constant, effects on each atom having non-zero magnetic moment. According to the above formula, each spin feels average magnetization derived from the other spins, primarily from the nearest neighbors. Analyzing the interactions between the atoms in the crystal lattice what should be considered are at least two of their origins: the attraction of the nuclear cores by a "sea" of conduction electrons (the effect of crystal field) and the electron exchange between orbitals of neighboring atoms (the effect of magnetism band). Each of these interactions leads to fracture spherical symmetry typical of isolated atoms and modifies the magnetic properties of the periodic system of polyatomic, thus determining their short- or long-range magnetic ordering.

Among the well-known schemes of exchange magnetic interactions, from the point of view of the analyzed system their magnetic structures are often the result of coexistence of several mechanisms mentioned below. For the continuity of this review I will describe some basic.

7.1 DIRECT EXCHANGE

The dominant interaction leading to the long-range order of magnetic moments is the direct exchange. The effect of the distancing of electrons of the same sign always lead to lowering system energy. If the energy of an electron pair i, j in the singlet state is denoted as E_s , and energy of triplet state as E_t , then the integral exchange J_{ij} in spin Hamiltonian $H = J_{ij} \cdot S_i \cdot S_j$ will be described by formula:

$$J_{ij} = \frac{E_s - E_t}{2} \quad (19)$$

Ferromagnetic coupling describes the positive exchange integral while the antiferromagnetic coupling describes the negative exchange integral. In the multielectron system all pairs of spins are taken into account what complicates Hamiltonian form $H = -2 \sum J_{ij} \cdot S_i \cdot S_j$ and effective exchange integral. Because the electrons interact with each other through spatial effective overlap of atomic orbitals, they occupy molecular orbitals. The measure of this efficiency is an overlap integral J_o and potential exchange integral J_p as well as J_h hopping integral, according to the equation:

$$J_{ij} = \frac{E_s - E_t}{2} = J_p - 2J_o J_h \quad (20)$$

In the case of $J_o = 0$ parallel spins orientation is preferred, but when $J_o \neq 0$ is so effective that $J_p < 2J_o J_h$ and thus potential exchange integral is less than the kinetic exchange term and a set of antiparallel spins is preferred. This is a direct exchange effect and the type of coupling is called as direct exchange interaction. The exchange mechanism is of the short-range order and rapidly weakens with increasing distance between interacting spins. Authorees set herself the question whether this is so important and so effective influence that together with a weaker long-range order in the powder samples it could lead to a blur out of the diffraction information about $\vec{q}_2 = (0.18, 0.18, 0)$? On the other hand, is it interaction strong enough to force the scandium atoms to take part in the magnetic ordering formation? But if it is not the primary interaction what are the other mechanisms to enforce slanted spin configurations of nearest neighbors or spin modulations and where should be seen the anisotropy sources?

7.2 RKKY INTERACTIONS

In a real systems the direct exchange is not the most important one, and often it cannot even be implemented because of too much distance r between magnetic ions and insufficient overlap of atomic orbitals. This is where an element, in which electrons of the $4f$ and less of $5f$

one, are strongly localized near the nucleus. In the case of transition metals Sc or Fe $3d$ orbitals are of greater extent. In cases mentioned above, the magnetic moments interact via the conduction electrons. This is an indirect exchange. The magnetic moment located on the atom polarizes the spins of the conduction electrons, which in turn influence on the moments of the neighboring atoms. Such a mechanism from authors' names Ruderman, Kittel, Kasuya and Yosida is further referred to as *RKKY* interaction. This long-range interaction depends on the density of states of the conduction electrons, and in the simplest model of interactions the exchange integral varies with the distance r in an oscillating manner in accordance with the formula:

$$J_{RKKY} \propto \frac{\cos(2k_F r)}{r^3} \quad (21)$$

where k_F is the Fermi vector. *RKKY* interaction leads to the long-range order and among other to the commensurate or incommensurate modulated magnetic structures observed mainly for elements of d - and f -electron.

As in described herein tetragonal cells with a large base and a small height, the main magnetic sublattice of a cuboid of approximate dimensions $(4.3 \times 4.3 \times 2.5)\text{\AA}^3$ is formed by iron atoms. The crystal unit cells are body centered in one case, by the poor d -electron scandium, and in the second one, by the poor f -electron uranium. In both systems, peculiar magnetic order was observed: in the scandium samples the incommensurate magnetic noncollinearity is present while the compound containing uranium discloses the commensurate magnetic noncollinearity only. In this context, using simulation algorithms described below, Authors tried to analyze the contribution of *RKKY* interactions that will influence the change of character and values of exchange integrals as a function of the distance of interacting atoms.

7.3 ANISOTROPIC EXCHANGE

Energy of exchange interactions types described above does not depend on the direction of the spins in the crystal lattice. In systems with uniaxial symmetry, when on the line connecting the magnetic ions there is no center of inversion, the spin - orbit (*SO*) interaction of one of the magnetic ions can cause the appearance of anisotropic exchange interaction, so-called Dzyaloshinskii–Moriya (*DM*) interaction. The interaction is defined by the vector D (usually $|D| \ll |J|$) parallel to the axis of symmetry. Coupling *DM* seeks to set the spins perpendicular to each other and to the vector D . As a consequence the weak ferromagnetic moment appears in antiferromagnetic system, as is in the case of UFe_4Al_8 or $ScFe_4Al_8$. The competitiveness of ferro - and antiferromagnetic interactions leads to noncollinear settings of

magnetic moments on (8*f*) iron sublattice what results that in the case of excess of scandium concentration the modulation vector slightly decreases. Similarly, the iron magnetic moment decreases by approximately of 30% in comparison to the value of 1.23 (6) μ_B /atom or 1.19 (8) μ_B /atom, depending on the domain in the ideal stoichiometric single crystal. During the analysis of polycrystalline systems close to 20% decrease of magnetic moment of iron of 1.08 (2) μ_B /atom in a stoichiometric sample to 0.87 (4) μ_B /atom in the arrangement with an excess of scandium concentration was observed. In contrast, the type of the neighbor residing at (2*a*) sublattice does not substantially affect on the angle of spins canting.

7.4 CRYSTAL FIELD AND ANISOTROPY IN TERMS OF THE MONTE CARLO METHODS

The algorithms used during Monte Carlo (*MC*) simulation together with Mean Field (*MF*) models are able to pinpoint the reasons for this and no other magnetic ordering in systems with weak anisotropy of a single ion. The general model, taking into account the anisotropy of the exchange interaction of modulated structures a consistent description of the experimental data in complex linkage model of spin - orbit (*SO*), *RKKY* and anisotropic *DM*-type interactions was achieved. Neglecting the effect of external magnetic field and having a Hamiltonian for ion in a solid state the expression with the contribution of Coulomb interaction type of electron-electron and electron-nucleus and the crystal field contribution and coming from the spin - orbit couplings was used:

$$\mathcal{H} = \mathcal{H}_c + \mathcal{H}_{cf} + \mathcal{H}_{so} \quad (22)$$

In the first *CF* models that were used to describe the properties of ionic crystals, the crystal field was identified with the electrostatic one derived from ions surrounding the magnetic atom. In the currently developed models (i.e. *Ab initio* calculations) it tries to describe the crystal field as an effective potential, with the main parameters: symmetry point of ambient magnetic ion and electron structure of closest neighbors, and here ambient symmetry is crucial. The influence of ambient symmetry on the electronic structure of magnetic ion is easier to understand by analyzing the shapes of *d*- and *f*- electron orbitals, as responsible for the magnetism of transition metal compounds and Actinides. Each of the *d* shell is composed of five orbitals of different shapes and spatial orientation while each of the *f* shell consists of seven orbitals of different shapes and spatial orientation. In the presence of a spherically symmetric potential the shell orbitals have the same energy, so it is a five-fold (*nd*) or seven-fold (*nf*) level degenerate. In the presence of the potential of lower point symmetry the shape and spatial orientation of the orbital cease to be indifferent to its potential energy. Various ambient symmetries may lead to different schemes of electron splitting levels. For this reason the determination of the ambient point symmetry is fundamental for

every CF model. Knowing this symmetry and basing on group theory it can be clearly defined the scheme of multiplet splitting, which as a data now is already tabulated. The problem in CF models is not the splitting way, but the distance on the energy scale between levels of split multiplet, because they depend on the electron structure. The scheme of splitting can be determined by spectroscopic methods. In the case of ambient point-symmetry for $4/mmm$ with a four-fold axis of symmetry and the c axis of quantization the crystal field (CF) describes the formula:

$$\mathcal{H}_{cf} = B_2^0 \hat{O}_2^0 + B_4^0 \hat{O}_4^0 + B_4^{4c} \hat{O}_4^{4c} + B_6^0 \hat{O}_6^0 + B_6^{4c} \hat{O}_6^{4c} \quad (23)$$

where B coefficients are CF parameters mutually correlated in the following manner:

$$B_{20} = -\frac{1}{2}B_2^0, \quad B_{40} = \frac{3}{8}B_4^0 + \frac{1}{8}B_4^4, \quad B_{44} = \frac{35}{8}B_4^0 + \frac{1}{8}B_4^4 \quad (23a)$$

while \hat{O}_{n+2}^n are the Stevens's operators. Only the second- and fourth-order terms exists for $3d$ ions ($l=2$), thus in the alloy of interest formula (23) simplifies to

$$\mathcal{H}_{cf} = B_2^0 \hat{O}_2^0 + B_4^0 \hat{O}_4^0 + B_4^{4c} \hat{O}_4^{4c} \quad (23b)$$

In turn, the term for spin-orbit coupling takes the form:

$$\mathcal{H}_{so} = \left(\frac{\Lambda}{\hbar^2}\right) \hat{L} \cdot \hat{S} \quad (24)$$

It remains to consider the problem of the anisotropy. Obviously, the magnetocrystalline anisotropy in the system is caused by the energy that is, for example, responsible for the appearance in ferromagnetic system the distinguished crystallographic directions, called directions of easy magnetization. This energy is called the energy of anisotropy or magnetocrystalline energy. Its origin cannot be explained by considering only isotropic exchange interaction. One source of magnetocrystalline anisotropy is an asymmetry in the overlapping electrons distributions of neighboring ions, where due to the spin-orbit interaction of electron the charge density distribution has an ellipsoidal shape. The asymmetry is associated with the direction of the spin: the spin rotation relative to the axis of the crystal changes the exchange energy and further energy of electrostatic interaction between the charge distributions of pairs of atoms. In the ‘‘simulation’’ papers [H6, H7, H8] the construction of the spin Hamiltonian of ScFe_4Al_8 system was based initially on eight atoms of magnetic iron. In the next step Hamiltonian was already based on the 10 atoms involved in the formation of magnetic ordering. The aluminum atoms were only treated as ‘nonmagnetic’.

Table 3. Nearest neighbors of the Fe₁: (1/4, 1/4, 1/4) in sets of both iron magnetic orbits as a result of the magnetic scattering vectors type $\tau_i = (\tau_{xi}, \tau_{yi}, 0) = (\tau_i, \tau_i, 0)$, where $i = 1, 2$ simultaneously, with the α - canting angle. In the case of scandium sublattices the collinear and commensurate ferromagnetism is assumed. In order to simplify the discussion of minimizing energy (presented at next chapter, H7) the appropriate phases of all magnetic atoms at starting magnetic unit cell (listed at 3rd column) are shifted by \vec{T} translation vector.

| Orbit | Atomic position \vec{r} translated by $\vec{T} = (\frac{1}{4}, \frac{1}{4}, \frac{1}{4})$ | Experimental phase | Appropriate distance with respect to Fe ₁ $ \vec{r} (pm)$ |
|------------------|---|---------------------------------------|--|
| 1 ⁰ | 1: (1/4, 1/4, 1/4) - T = (0,0,0) | $\varphi_1 = \alpha + \pi\tau$ | 0.0 |
| | 2: (1/4, 1/4, 3/4) - T = (0,0, 1/2) | $\varphi_1 = \alpha + \pi\tau$ | 249.9 |
| | 3: (3/4, 3/4, 3/4) - T = (1/2, 1/2, 1/2) | $\varphi_2 = \alpha + 3\pi\tau$ | 657.6 |
| | 4: (3/4, 3/4, 1/4) - T = (1/2, 1/2, 0) | $\varphi_2 = \alpha + 3\pi\tau$ | 608.26 |
| 2 ⁰ | 5: (1/4, 3/4, 3/4) - T = (0, 1/2, 1/2) | $\varphi_3 = \pi - \alpha + 2\pi\tau$ | 497.43 |
| | 6: (3/4, 1/4, 3/4) - T = (1/2, 0, 1/2) | $\varphi_3 = \pi - \alpha + 2\pi\tau$ | 497.43 |
| | 7: (3/4, 1/4, 1/4) - T = (1/2, 0, 0) | $\varphi_3 = \pi - \alpha + 2\pi\tau$ | 430.1 |
| | 8: (1/4, 3/4, 1/4) - T = (0, 1/2, 0) | $\varphi_3 = \pi - \alpha + 2\pi\tau$ | 430.1 |
| Sc _I | I: (0,0,0) - T = -(1/4, 1/4, 1/4) | $\varphi_4 = 0$ | 328.8 |
| Sc _{II} | II: (1/2, 1/2, 1/2) - T = (1/4, 1/4, 1/4) | $\varphi_4 = 0$ | 328.8 |

In view of the rather poor information concerns basic parameters determined from computational models such *CF* coefficients, Stevens's operators, exchange integrals at the level of J_{dd} , J_{df} or J_{ff} molecular orbitals, the replacing of atoms by magnetic ions have been made (Table 1 of paper H6), especially during analysis of spin-orbit interactions within the *MCPPhase* algorithm. In the next part thee detailed potential possibilities for each of the simulation packages will be described, but some fundamental differences have been presented in Table 4.

Table 4. Comparison of the assumptions made during Monte Carlo calculation.

| <i>MCMag</i> | <i>MCPPhase</i> |
|---|---|
| Spins are treated classically | Spins are treated quantum-mechanically |
| $\mathcal{H} = \mathcal{H}_{cf} + \mathcal{H}_{DM}$ | $\mathcal{H} = \mathcal{H}_{cf} + \mathcal{H}_c + \mathcal{H}_{so}$ |
| $\mathcal{H}_{cf} = \sum_S D_x^2 (J_x)^2 + D_y^2 (J_y)^2 + D_z^2 (J_z)^2$ or $\mathcal{H}_{cf} = \sum_S D_z^2 (J_z)^2 - K_{xy}^2 [(J_x)^2 - (J_y)^2]$ and $\mathcal{H}_{DM} = A\vec{n}(\vec{J}_1 \times \vec{J}_2)$ | $\mathcal{H}_{cf} = \sum_{n,l,m} B_l^m O_l^m (J^n)$, where $O_2^0 = 3(J_z)^2 - X$, $O_4^0 = 35(J_z)^4 - (30X - 25)(J_z)^2 + 3X^2 - 6X$, $O_4^4 = \frac{1}{2}(J_+^4 + J_-^4)$ for $X = J(J + 1)$ and $\mathcal{H}_{so} = \left(\frac{\Lambda}{\hbar^2}\right) \hat{L} \cdot \hat{S}$ |
| Exchange constants J_{ij} have be postulated and stiffened during calculations. | Exchange constants J_{ij} may be a variable parameters during calculations. |

The basic input data to both of the programs is a microscopic description of the measured system, i.e. a list of magnetic sublattices with spins's amplitudes and the description of the relations between sublattices by the corresponding exchange integrals and finally the Hamiltonian's form, which will be used for calculation of the system energy. For example, the general form of the Hamiltonian used in the *MCMag* describes the formula:

$$E = -\frac{1}{2} \sum_{\langle i,j \rangle} \vec{S}_i [J_{ij}] \vec{S}_j + \frac{\sum_i (\vec{D}_i \vec{S}_i)^2}{|D_i|} - \sum_i \vec{H} \vec{S}_i \quad (25)$$

where S_i, S_j are the vectors of interacting spins, J_{ij} - a coupling tensor D_i is the vector of the anisotropy of a single ion, while H is the vector of the applied magnetic field.

There may be a difference in the boundary conditions, e.g. in the *MCMag* appropriate numerical codes mean free edges, periodic boundary conditions, or mixed conditions typical for incommensurate structures. However, in *MCPPhase* modulation vector of value $0.133 = \frac{2}{15}$ was used as input data, and therefore the periodicity of magnetic cells is: $15 \times 15 \times 1 = 225$ crystal cells and of $15 \times 15 \times 8 = 1800$ the atoms. By using the *MC* in a technical manner, the simulations start at some high temperature, where the spins are dynamically disordering ('liquid state'). Configurations of the ground state are obtained by the Metropolis-Hastings algorithm of simulated cooling $T(n + 1) = \alpha \cdot T(n)$ [16^{xvi}, 17^{xvii}].

The new orientation (spin configuration) is projected at random, then accepted or rejected: the multi-spins system creates different configurations for different energies. In fixed temperature T and in n^{th} iteration of cooling scenario the probability of finding a given energy $E_n = \Delta E + E_{n-1}$ is proportional to the Boltzmann factor of form $e^{\frac{-E}{kT}}$. The convergence criterion is the energy minimization. Thus the spin configurations of the energy E_n higher than the energy configuration optimized in the previous iteration E_{n-1} are rejected. This process is repeated many times (cycles *Monte Carlo*) until the system reaches the equilibrium. Then the temperature is lowered, the spin system will search a new equilibrium again, and so on. The reference system used for the projection of the spin is completely independent of crystallographic one. The new spin configurations are always generated and expressed in an orthogonal coordinate system. The same orthogonal coordinate system is used to determine the coefficients of anisotropy and the magnetic field, if any. After the simulation the projection of the magnetic moments with the turnover of the spin system configuration with respect to the reference crystal one is generated. This option makes it easier to compare the result of simulation and real spins configuration. External simulation conditions (cooling story or screenplay magnetic) are entered interactively (via dialog boxes). If the protocol of cooling or heating one is executed enough carefully, the system will run away from the local energy minima and determine the spin configuration with the lowest energy.

Averaged characteristics of the magnetic susceptibility and specific heat, energy of the spin configuration or the magnetization are recorded and collected in each iteration. During *MCMag* cycles appropriate agreements factors can be traced: (i) so-called rate of accepted jumps and (ii) the constraint function - F_c - which is a measure of the degree of frustration of a magnetic structure. The rate of accepted jumps is the rate of acceptance of new spin configurations at a given temperature and field. Obviously, the rate of accepted jumps takes into account any new spin configuration that is identical to the old one. The constraint function is defined as:

$$-1 \leq F_c = - \sum_{\langle ij \rangle} J_{ij} \vec{S}_i \vec{S}_j / \sum_{\langle ij \rangle} |J_{ij}| |\vec{S}_i| |\vec{S}_j| \leq 1 \quad (26)$$

and it works in a range from not frustrated magnetic structures ($F_c = -1$) after completely frustrated ($F_c = 1$). *MCMag* program is a powerful tool for simulations of magnetic ordering, able for searching izoenergetic spin configurations, reversible magnetization characteristics in the cooling and heating system scenario and the coupling constants. Configuration space is examined by random sampling using the Metropolis [17^{xvii}] procedure. Any magnetic structure can be simulated without any constraints of interaction distances. In the first step the magnetic supercell of ScFe_4Al_8 comprising $3 \times 3 \times 1$ crystal cells was analyzed. The spins of iron lay in the base ab plane of the tetragonal unit cell and they formed the canted structure, i.e. the predominant antiferromagnetic coupling in the direction of $[100]$ have been enriched with a weak ferromagnetic components on the direction $[010]$. Such a spin model required to

impose positive values of D anisotropy coefficients along the axis b and c and a negative D coefficient along the axis a . In further studies, all of the exchange integrals have been modified to the value obtained from the *MCPPhase*. The simulation started at room temperature from paramagnetic state. Input files contained the magnetic atoms, the structure data i.e. lattice parameters and angles without taking into account the symmetry elements, a list of neighbors and the appropriate exchange integrals, anisotropy coefficients and spin amplitudes.

MCPPhase package subroutines type of *searchspace* and *simannfit* (Figure 16) are used to search the exchange integrals in various areas in order to find local minima of the standard deviation function sta^3 . On this principle the whole map of exchange integrals is agreed. It starts with the initial map of the exchange integrals based on a histograms of all contemplated exchange constants, which minimize a function of the standard deviation sta (coupling constant A , ..., coupling constant K). By agreeing magnetic ordering in the framework of exchange integrals data the algorithm consistent with *Mean Field* approximation and *Monte Carlo* methods is used in the *mcpphas* module.

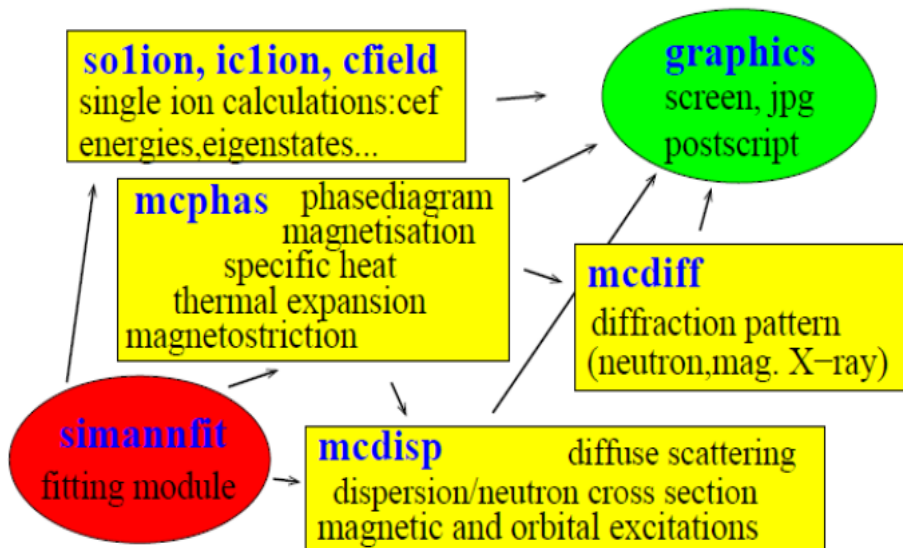


Figure 16. Scheme of *MCPPhase* software package, where a *silion* subprogram is dedicated to parametric descriptions of the properties of Lanthanide ions taking into account the hierarchy

³ If the function $\exp\left(\frac{sta(newA...) - sta(A...)}{T}\right) < a$ where the random variable a comes from the interval [0,1] the step of change is accepted, if not – rejected. Minimized during computing cycle variance $s^2 = \frac{1}{N} \sum_i \delta_i^2$ contains to a dozen N divisions of previously defined interval of variation of each variable function $sta = \delta_i^2$.

of the Coulomb interaction and the spin-orbital as well as crystal field influence, in this case $H_c \gg H_{so} \gg H_{cf}$. The *icflion* subroutine allows to parameterize transition metal ions ($H_c \sim H_{cf} \gg H_{so}$), while *iclion* allows to parameterize Actinide ions ($H_c \sim H_{so} \sim H_{cf}$).

At a given temperature and at a given magnetic field vector the several equally probable magnetic structures is stabilized by *MF* algorithm and the free energy is calculated. Moreover, thanks to *mcpas* subroutine all components of the magnetic moment are obtained and then the izoenergetic spin configurations and modulation vectors are recalculated. According to Monte Carlo calculations the maps of exchange constants which give the best reconstructions of the spin configurations are associated with the standard deviation $sta=0.16$ in the case of \vec{q}_1 mode and $sta=0.22$ for \vec{q}_2 one.

During calculations relevant dynamic characteristics are displayed on the screen. The intensities of neutron reflections (*hkl*) as a function of temperature and magnetization curves characteristics can be compared to those obtained experimentally.

Table 5. The bilinear magnetic tensors dedicated to (8f) positions of the space group *I4/mmm*. DM interactions were taking into account. The meanings of ‘orbits’ is given earlier in Figure 10.

| No. | Exchange tensor $\vec{J}(nn')$ | Distance $r_{n'} - r_n$ |
|-----|---|--|
| 1 | $\begin{bmatrix} A & A & 0 \\ A & A & 0 \\ 0 & 0 & 0 \end{bmatrix}$ | $\begin{pmatrix} 0 \\ 0 \\ \pm c/2 \end{pmatrix}$ |
| | ‘between-orbits’ tensors | |
| 2 | $\begin{bmatrix} -B & -D & 0 \\ D & C & 0 \\ 0 & 0 & 0 \end{bmatrix}$ | $\begin{pmatrix} 0 \\ b/2 \\ 0 \end{pmatrix} \text{ and } \begin{pmatrix} 0 \\ b/2 \\ \pm c/2 \end{pmatrix}$ |
| 3 | $\begin{bmatrix} -E & -G & 0 \\ G & F & 0 \\ 0 & 0 & 0 \end{bmatrix}$ | $\begin{pmatrix} 0 \\ -b/2 \\ 0 \end{pmatrix} \text{ and } \begin{pmatrix} 0 \\ -b/2 \\ \pm c/2 \end{pmatrix}$ |
| 4 | $\begin{bmatrix} -H & -K & 0 \\ K & I & 0 \\ 0 & 0 & 0 \end{bmatrix}$ | $\begin{pmatrix} a/2 \\ 0 \\ 0 \end{pmatrix} \text{ and } \begin{pmatrix} a/2 \\ 0 \\ \pm c/2 \end{pmatrix}$ |

| | | |
|---|---|--|
| 5 | $\begin{bmatrix} -E & -G & 0 \\ G & F & 0 \\ 0 & 0 & 0 \end{bmatrix}$ | $\begin{pmatrix} -a/2 \\ 0 \\ 0 \end{pmatrix} \text{ and } \begin{pmatrix} -a/2 \\ 0 \\ \pm c/2 \end{pmatrix}$ |
| | ‘in-orbits’ tensors | |
| 6 | $\begin{bmatrix} -H & -K & 0 \\ D & C & 0 \\ 0 & 0 & 0 \end{bmatrix}$ | $\begin{pmatrix} a/2 \\ b/2 \\ 0 \end{pmatrix} \text{ and } \begin{pmatrix} a/2 \\ b/2 \\ \pm c/2 \end{pmatrix}$ |
| 7 | $\begin{bmatrix} -E & -G & 0 \\ G & F & 0 \\ 0 & 0 & 0 \end{bmatrix}$ | $\begin{pmatrix} \pm a/2 \\ \mp b/2 \\ 0 \end{pmatrix} \text{ and } \begin{pmatrix} \mp a/2 \\ \pm b/2 \\ \pm c/2 \end{pmatrix}$ |

Table 6. Considering the interactions around the atom 1: (1/4, 1/4, 1/4) (as shown in Figure 17) the calculated exchange constants for the noncollinear τ_1 and τ_2 configurations at the temperature range 1-31K (*McPhase*), in which the interactions are relatively strong, are as follows. The exchange integrals are coded as adopted earlier by the notation of bilinear magnetic tensors (Table 5).

| | $J_{[001]}$ | $J_{[100]}$ | $J_{[010]}$ | | $J_{[100]}$ | $J_{[010]}$ | | $J_{[100]}$ | $J_{[010]}$ | |
|--------------------|-------------|-------------|-------------|------|-------------|-------------|------|-------------|-------------|------|
| J [meV] | A | B | C | D | E | F | G | H | I | K |
| $\tau_1 - McPhase$ | 0.38 | 0.85 | 0.66 | 0.59 | 0.87 | 0.45 | 0.68 | 0.78 | 0.69 | 0.71 |
| $\tau_2 - McPhase$ | 0.38 | 1.11 | 0.66 | 0.77 | 0.96 | 0.45 | 1.22 | 0.55 | 0.69 | 0.71 |
| $\tau_1 - McMag$ | 0.38 | 1.44 | 0.72 | 1.41 | 1.22 | 0.50 | 0.48 | 0.94 | 0.69 | 0.64 |
| $\tau_2 - McMag$ | 0.52 | 1.53 | 0.66 | 1.76 | 1.30 | 0.72 | 1.02 | 1.01 | 1.24 | 0.92 |

Looking at the exchange integrals between atoms lying along [100] (appropriate tensors no. 5 and 4 on Table 5), [010] (tensors no. 3 and 2) and [001] (tensors no. 1) directions it seems to be interesting to compare them with well – known exchange integrals typical for the canting $\beta-MnO_2$ structure of the rutile type [18^{xviii}] where by assuming $J_{[001]}/J_{[111]} = -1.60$: $J_{[001]} = -0.767$ meV, $J_{[111]} = 0.474$ meV and $J_3 = -0,112$ meV, where $J_{[001]}$ is the exchange

integral between nearest neighbors (in the $\langle 001 \rangle$ direction), $J_{[111]}$ acts between next nearest neighbors ($\langle 111 \rangle$ direction) and J_3 refers to third- neighbor coupling respectively (Figure 17). Noteworthy, that a sequence of integrals J [100] (framed in green rows of Table 6) clearly shows the oscillating behavior of the *RKKY* interaction.

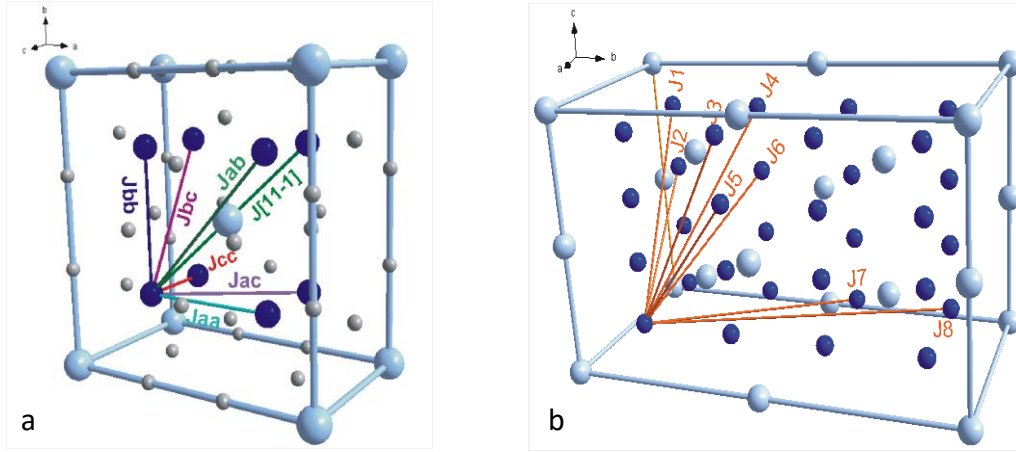


Figure 17. The exchange integrals in basic ‘0th’ unit cell (a) which from point of view crystal periodicity leads to 14 nn (under assumption of the distance to nearest neighbours so-called $m_{kenn} = 500$ pm – *MCP* phase parameter) and in the next step 26 nn was considered, which corresponds to $3 \times 3 \times 3$ – *MCM* mag or $m_{kenn} = 1000$ pm – *MCP* phase, respectively. In the case of a closing in spin wave associated with the modulation $\vec{q}_2 = (\pm 0.18, \pm 0.18, 0)$ 32 nn is required (b).

In the case of the crystal containing scandium is not surprising twice lower value of the exchange integral along [001] direction in relation to the corresponding integral in the rutile structure, where the distances between nearest magnetic neighbors are much lower (~ 150 pm). Similarly, it is not surprising a positive sign of it, because in this direction in MFe_4Al_8 systems atoms usually interact ferromagnetically with each other. The contribution of scandium ions to the magnetism of the sample is still a problem. In particular, the interactions with the Sc ions in conjunction with the effects of anisotropy of Dzyaloshinskii–Moriya and dipole-dipole origin may assist the anisotropy effects. Therefore, the effort to check the effect of the small magnetic moment assigned to scandium atom has been made. Starting from zero to a value of $0.023 \mu_B/\text{atom}$ along [010] direction is known that such a modification of the magnetic model not lead to changes in the magnetization characteristics at low temperatures obtained from the *MCM* mag program in the accepted scenario of heating.

During heating at the temperature range 0 - 400 K in accordance with the Hastings - Metropolis algorithm magnetic order was checked in 63 measuring points ($\alpha = 1.1$). The complete closed cycles, i.e. cooling which followed after heating with the step of $\Delta T = 5K$ is illustrated in Figure 6 of paper [H6]. The model with adopted (2a) positions - on the similarity to UFe_4Al_8 - commensurate collinear ferromagnetism was adopted to *MC* calculation. In spite of simplicity of the proposed description of the exchange constants maps the results are encouraging.

8 RECONSTRUCTION OF THE EXCHANGE INTEGRALS MAP OF $SCFe_4Al_8$ MAGNETIC STRUCTURE [H7]

During simulations and calculations presented below the distance of the exchange interactions was restricted up to 430.1pm (6nn). Were the iron spins ordered ferromagnetically, the observed transition temperatures $T_1 \sim 230K$ and $T_2 \sim 115K$ [H2, H3] would, at the first step, correspond to exchange integrals close to $J_1 \sim 20 meV$ and $J_2 \sim 10 meV$, respectively. As a dominant terms of Hamiltonian the exchange interactions J_{Fe-Fe}^{RKKY} with $k_F = 0.5 \text{ \AA}^{-1}$ were considered.

Taking into account 6 nn, it faces the problem of energy minimization which is described by formula:

$$E = -8S^2(J_{aa} + J_{bb}) \cos \pi\tau [\cos^2 \pi\tau - \sin^2 \alpha] + 6S^2 J_{cc} \quad (27)$$

Thus,

$$\left. \begin{aligned} \partial E / \partial \tau &= 8\pi S^2 (J_{aa} + J_{bb}) (3 \cos^2 \pi\tau - \sin^2 \alpha) \sin \pi\tau \\ \partial E / \partial \alpha &= 8S^2 (J_{aa} + J_{bb}) \sin 2\alpha \cos \pi\tau \end{aligned} \right\} \quad (28)$$

Next the incommensurability and noncollinearity dependence on the position of energy minima leads to the simple relations: $\partial E / \partial \tau = 0 \Rightarrow \tau = 0$ (experimentally rejected) or $3 \cos^2 \pi\tau = \sin^2 \alpha$ and $\partial E / \partial \alpha = 0 \Rightarrow \tau = 1/2$ requires $(2a \times 2a \times c)$ magnetic unit cell or $\sin 2\alpha = 0 \Rightarrow \alpha = 0, \pi/2$. Such terms refer to the collinear structure (modulation type magnetic $\vec{q}_1 = (\pm 0.13, \pm 0.13, 0)$) or to an orthogonal magnetic moments distribution (such distribution was estimated within the domain).

$$\left. \begin{aligned} \partial^2 E / \partial \tau^2 &= 8\pi^2 S^2 (J_{aa} + J_{bb}) \cos \pi\tau [9 \cos^2 \pi\tau - \sin^2 \alpha - 6] > 0 \\ \partial^2 E / \partial \alpha^2 &= 16S^2 (J_{aa} + J_{bb}) \cos 2\alpha \cos \pi\tau > 0 \end{aligned} \right\} \quad (29)$$

finally,

$$\cos\pi\tau > 0 \text{ and } 9 \cos^2 \pi\tau - \sin^2\alpha > 6, \cos\pi\tau > 0 \text{ and } \cos 2\alpha > 0 \quad (30)$$

For a given temperature several possible magnetic structures are usually stabilized and the free energy is calculated. For stable structures all components of the magnetic moment have to be obtained. The *MCPhase* procedure leads to less anisotropic interactions ($B=H$, see Table 1 of H7 paper) with the resultant magnetic moment $1.38 \mu_B/\text{atom}$ stable up to $T=11\text{K}$ (*MCPhase*) with mostly weaker exchange constants while *MCMag* calculations let imitate $1 \mu_B/\text{atom}$ stable up to $T=51\text{K}$. The exchange constants obtained by use *McPhase* program leads to slightly overestimated intensities of the magnetic satellites observed in neutron scattering (Figure 18). The reasons are: (i) calculated iron magnetic moment larger than the experimental one, (ii) the *RKKY* and *DM* interactions only are taken into account.

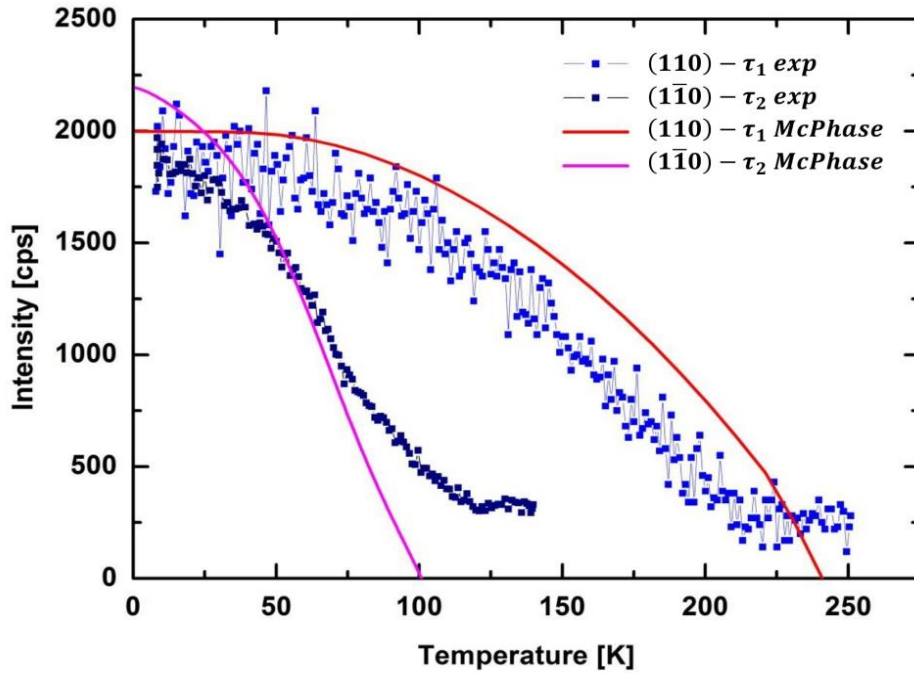


Figure 18. Thermal variation of the integrated neutron intensities of the strongest magnetic satellites obtained experimentally and during *McPhase* calculations of simulated cooling for the case of 14 nm.

The map of the exchange integrals were reconstructed. We have shown, that the dominant antiferromagnetic interactions between iron atoms should be treated as of *RKKY+DM* origin. In spite of the complexity of the proposed description, the obtained results are encouraging.

For several years, the magnetic ordering UFe_4Al_8 was interpreted in a variety of often excluding manner. Finally, thanks to techniques using polarized and non-polarized neutron two magnetic subnet has been accurately recognized. Uranium sublattice ($2a$) reveals the collinear ferromagnetism but remains highly noncollinear (almost orthogonal) with respect to the iron sublattice ($8f$). Iron sublattice itself is also noncollinear here because instead of G - type antiferromagnetism a spin-canted system with a lower component of ferromagnetic Fe moments directed parallel to the U moments is formed. The uranium compound reveals two types of noncollinearity. The problem turned out to be so enigmatic that attempts have been made in order to gain the interest of theoretical groups initiating electronic structure calculations of the UFe_4Al_8 structure, as the simplest one in the MFe_4Al_8 family. The monograph [H3] was to serve as a compendium of the most important properties of the described spin structures and thus inspire the band structure calculations, unfortunately without success. Represented here Hamiltonian was based on the 10 atoms which are responsible for the magnetic ordering formation.

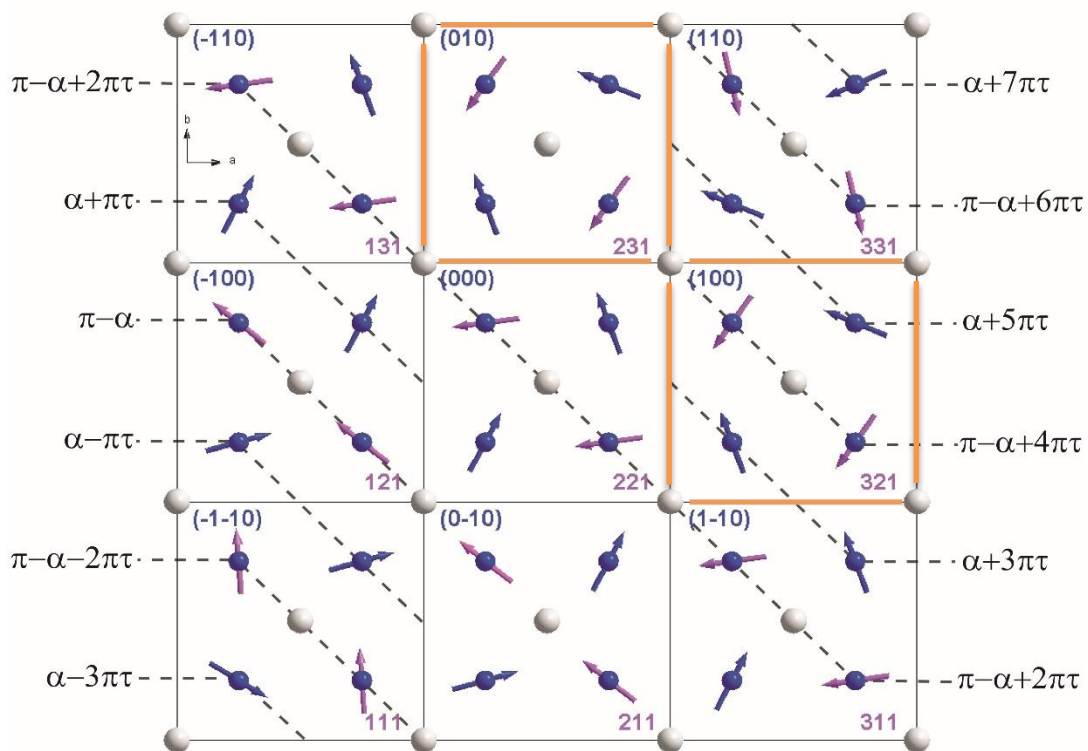


Figure 19. 2D schematic representation of the iron moment arrangement in the ab plane containing the wave vector $(\tau_i, \tau_i, 0)$ – the case of the (8f) sublattice of ScFe_4Al_8 magnetic structure – which locks-in to $(0,0,0)$ at 231 or 321 cells – the case of the (8f) sublattice of UFe_4Al_8 magnetic structure, respectively.

The commensurability of UFe_4Al_8 system with regard to the incommensurability of ScFe_4Al_8 was analyzed based on the Heisenberg's Hamiltonian. The terms related to the Dzyaloshinskii–Moriya, Ruderman-Kittel-Kasuya-Yoshida as well as dipole interactions were taken into account in the model. These three types of interactions are treated as a probable origins of magnetocrystalline anisotropy in family of ThMn_{12} compounds. The calculated values and directions of the magnetic moments by use of neutron diffraction data are compared to those obtained experimentally, starting from the configuration of the ground state by algorithm of simulated cooling. "Freezing" magnetic modulation observed in the case of (2a) sublattice of uranium sample (Figure 19) is analyzed using the appropriate exchange integrals relations. In the case of the uranium - in two ways noncollinear system - thoroughly analyzed also the canting angle as a function of the relationship of exchange integrals. This analysis showed poor accordance with the experiment range of accepted values.

The general expression for energy which is correct for the (8f) sublattice of incommensurate systems and noncollinear at both sublattices namely (8f) and (2a):

$$E = -6S_{Fe}^2 \{J_{aa} \cos(\varphi_3 - \varphi_1) + J_{aa} \cos(\varphi_3 - 2\pi\tau - \varphi_1) + J_{bb} \cos(\varphi_3 - \varphi_1) + J_{bb} \cos(\varphi_3 - 2\pi\tau - \varphi_1) + 2J_{cc}\} - 7S_{Fe}^2 \{J_{ab} \cos(\varphi_2 - \varphi_1) + J_{\bar{a}\bar{b}} \cos(\varphi_2 - 2\pi\tau - \varphi_1) + J_{a\bar{b}} + J_{\bar{a}b} + 2J_{ac} \cos(\varphi_3 - \varphi_1) + 2J_{a\bar{c}} \cos(\varphi_3 - 2\pi\tau - \varphi_1) + 2J_{bc} \cos(\varphi_3 - \varphi_1) + 2J_{b\bar{c}} \cos(\varphi_3 - 2\pi\tau - \varphi_1)\} - 4S_{Fe}S_{Sc} \{J_{abc} \cos(\varphi_4 - \varphi_1) + J_{\bar{a}\bar{b}c} \cos(\varphi_4 - \varphi_2) + (J_{a\bar{b}c} + J_{\bar{a}bc}) \cos(\varphi_4 - \varphi_3)\} \quad (31)$$

The above expression is discussed in view of the minimization of the energy system:

$$\partial E / \partial \alpha = -24S_{Fe}^2 (J_{aa} + J_{bb}) \sin 2\alpha - 112S_{Fe}^2 J_{ac} \sin 2\alpha - 16S_{Fe}S_U J_{abc} \cos \alpha \quad (32)$$

Another condition of energy minimization which examines noncollinearity of the magnetic structure:

$$\partial E / \partial \alpha = 0 \Rightarrow -S_{Fe} \sin \alpha [3(J_{aa} + J_{bb}) + 14J_{ac}] = S_U J_{abc} \quad (33)$$

hence

$$\frac{S_U}{S_{Fe}} = - \frac{[3(J_{aa} + J_{bb}) + 14J_{ac}] \sin \alpha}{J_{abc}} \quad (34)$$

therefore

$$3(J_{aa} + J_{bb}) + 14J_{ac} = - \frac{S_U J_{abc}}{S_{Fe} \sin \alpha} \quad (34a)$$

$$\partial^2 E / \partial \alpha^2 = -48S_{Fe}^2(J_{aa} + J_{bb})\cos 2\alpha - 224J_{ac}\cos 2\alpha + 16S_{Fe}S_U J_{abc}\sin \alpha > 0 \quad (35)$$

finally,

$$S_{Fe}[3(J_{aa} + J_{bb}) + 14J_{ac}]\cos 2\alpha < S_U J_{abc}\sin \alpha \quad (36)$$

$$\frac{[3(J_{aa}+J_{bb})+14J_{ac}]\cos 2\alpha}{J_{abc}\sin \alpha} < \frac{S_U}{S_{Fe}} \quad (37)$$

Considering both conditions minimizing the energy of the system (equation 34a and 37) the common solution corresponds to the relationship:

$$\frac{\left[\frac{-S_U J_{abc}}{S_{Fe}\sin \alpha}\right]\cos 2\alpha}{J_{abc}\sin \alpha} < \frac{S_U}{S_{Fe}} \quad \text{and next} \quad \cos 2\alpha < \sin^2 \alpha \quad (38)$$

Thus the stable UFe_4Al_8 spin-canted structure is predicted for canting angles $\pi/5 < \alpha \leq \pi/2$ and from eq. (34a) finally can be obtain relation:

$$J_{aa} + J_{bb} = -5 \left(\frac{J_{abc}}{8} \frac{S_U}{S_{Fe}} + J_{ac} \right) \quad (39)$$

The above conditions are weakly consistent with the experimental results, where [H2] $\alpha \leq \pi/6$ was reported. On the other hand, the strongest in-phase scattering was observed along diagonals what leads to prediction of the positive signs of J_{ac}, J_{abc} thus $J_{aa} = -J_{bb}$ is the only consistent condition and undoubtedly resulted in *DM*-type anisotropy. A similar approach to obtain the basic relations between exchange constants has been made for $ScFe_4Al_8$ [H7]. Obviously, due to conditional solutions of the exchange constants without extra dependences presented here equations are too complicated and it can only resolve them by use Monte Carlo methods.

Using both of the above-described Monte Carlo simulation packages attempt was made to reconstruct the magnetic structure confirmed experimentally. Two important differences in the assumptions made in the model used in both packages are worth emphasizing: (1) different formulas of Hamiltonian equations and (2) a much more detailed description of anisotropy of a single ion, ability to use (but not always justified) iso-electronic configuration, e.g. Ni^{2+} instead of Fe^0 or V^{2+} instead of Sc^0 as well as the freedom of choice of $U^{3+} (5f^3)$ instead $U^{4+} (5f^2)$ offered by the *MCPPhase* program.

Table 7. The solution of bilinear magnetic tensors dedicated to 6nn of each i -th iron atom located at $(8f)$ positions of the $I4/mmm$ space group, taking into account DM interactions where the appropriate vectors $\overline{r_i - r_j}$. The elements of the square matrix are shown in the 3th and 4th column. Tensor parameter designations remain in accordance with the scheme set out in Table 5.

| Exchange tensor parameters | $(r_i - r_j)/pm$ | MCP_{hase} $J_{ij}[meV]$ | MCM_{ag} $J_{ij}[meV]$ |
|----------------------------|---|-------------------------------|-----------------------------|
| A | $\begin{pmatrix} 0 \\ 0 \\ \pm 251.5 \end{pmatrix}$ | 0.46 | 0.03 |
| B(-) | $\begin{pmatrix} 0 \\ 436.8 \\ 0 \end{pmatrix}$ | 1.14 | 2.011 |
| C | | 0.63 | 1.66 |
| D(\pm) | $\begin{pmatrix} 0 \\ -436.8 \\ 0 \end{pmatrix}$ | 1.36 | 2.111 |
| E(-) | $\begin{pmatrix} 436.8 \\ 0 \\ 0 \end{pmatrix}$ | 0.98 | 1.31 |
| F | | 0.99 | 1.05 |
| G(\pm) | $\begin{pmatrix} -436.8 \\ 0 \\ 0 \end{pmatrix}$ | 1.19 | 1.54 |

In the case of a system containing uranium - doubly noncollinear - the values of canting angle was considered in terms of the exchange integrals ratios. Successful reconstruction the spin arrangement based on exchange integrals and phase transition temperatures at a level of commensurate structure or with a single modulation was achieved. Consistently with experimental results, one does not observe the lowering of resultant moments on the iron atom below $0.87 \mu_B$ and $1.46 \mu_B$, respectively. However the compatibility of the relationship of the obtained exchange integrals is much worse: $-1.2_{MCM_{ag}} > \frac{J_{aa}}{J_{bb}} > -1.8_{MCP_{hase}}$ and $-67_{MCM_{ag}} < \frac{J_{aa}}{J_{cc}} < -2.5_{MCP_{hase}}$. The Monte Carlo calculations indicate for the strongest exchange interaction along a -direction and of a different type than along the other two orthogonal directions. The weakest exchange interactions can be seen in the c -direction.

Particularly weak interactions J_{cc} i.e. about 67 times fainter in relation to dominating J_{aa} were obtained in the course of calculations using *MCMag* package. In contrast, the relationship of J_{aa} to J_{bb} are comparable in absolute values (according *MCMag*) although at the direction of b are almost twice weaker compared to the strongest exchange constants (by *MCPPhase*). This result agrees poorly with the experiment range of accepted values of canting angle. Namely, stable spin-canted structure is provided for canting angles in the range of $\pi/5 < \alpha \leq \pi/2$, while the results of experiments indicate on the canting angle $\alpha \leq \pi/6$. The strongest coherent neutron scattering was observed along the diagonal [110] which leads to expectations of positive signs of integrals J_{ac}, J_{abc} . While the relationship $J_{aa} = -J_{bb}$ without doubt stems from *DM* anisotropy.

It must be remembered that strongly correlated states of *5f* electrons in the intermetallic compounds of Actinides are not the same as the states of individual, free electrons. The intra-atomic Coulomb interaction, spin-orbit interaction and crystal field are probably stronger than the energy of interatomic hopping of *f-f* or *d-f*. In this case, it is reasonable to start with a fully localized or well-described crystal field states *f*, and then add the appropriate contributions of hopping energy and thus achieving a faithful description of the degree possible 'itinerancy' of electrons. In the case of intermetallic compounds of Actinide the signs and values of the parameters of the crystal field are unknown. Moreover, in the description of crystal field the ground state of configuration $5f^2$ it is a non-magnetic singlet state. To test the importance of all these approximations or inconsistencies the inelastic neutron scattering experiments on single crystals as well as *ab-initio* calculations of phonon dispersion law should be performed.

10 MAGNETIZATION DISTRIBUTION IN NONCOLLINEAR MAGNETIC SYSTEMS WITH MUTUALLY PERPENDICULAR CRYSTAL AXES [H9]

Physical and chemical system properties are typically fully defined by the distribution of electron density in the system in accordance with Hohenberg - Kohn theorem [19^{xix}] since 1964. Currently, there are used mainly two methods for determining the density distribution of electrons in a crystal: a) a multipole refinement and b) the maximum entropy method (*MEM*).

The first of these methods should be difficult to apply in the case of metal crystals. It is based on the knowledge of the electron wave functions: building a model of the unit cell of the atoms and each of which is described using a set of wave functions and adjusts only some of the parameters of this model. As a result, each atom accounts for tens of fitting parameters are often highly correlated each other, making the problem of complex numerically. Inserting information about the form of the wave function, it assumes roughly known the distribution of

electrons in the crystal. As a result, some of the properties such density diffusion regions, i.e. the interatomic areas on which is a higher electron density may be invisible in this model. As demonstrated by Bruning [20^{xx}] multipole model is unable to describe the diffusion areas loads in the crystal. In conclusion, during multipole refinement method, the key is the information inserted at an early stage of building a model. Separately are treated electrons of the core and valence electrons. The distribution of these former is consider as known - spherically symmetric and the wave functions of valence electron are modifications only . A disadvantage of multipole models is that the properties of the charge density distribution which has not previously been "programmed" in this model, it never did not occur [21^{xxi}].

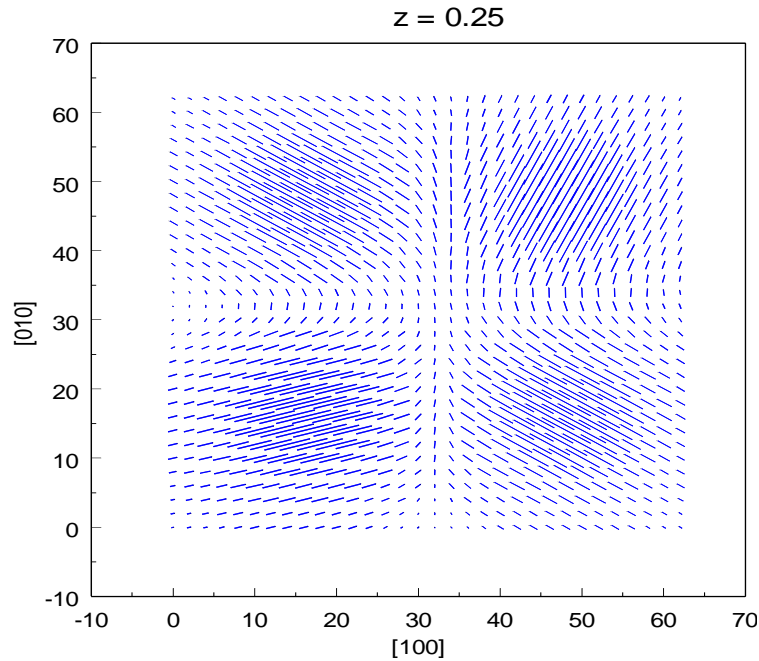


Figure 19. The magnetization density distribution in xy plane for $z=0.25$ coordinate. The every second point in each direction was shown for better readability. The length of the magnetization vectors are given in a logarithmic scale. The magnetization changes in the region from $0.0 \mu_B/\text{\AA}^3$ to $1.45 \mu_B/\text{\AA}^3$.

MEM method is a without-model method. What is bad, is the fact that this method determines both the distribution of all the electrons as the core and valence, and because the density of valence electrons are tenth per cent of electron density core of core electrons, it is natural that obtained by this method the density of valence electrons may be subject to considerable uncertainty. In turn, the distribution of magnetization is bound to valence electrons only. In consequence the results of examination of the magnetization distribution may be used to obtain the proper valence electron density distribution, free from defects

introduced by the previous method. Thus the magnetization distribution can be a source of an accurate information about the distribution of valence electrons in the unit cell that are involved in the formation of bonds between atoms in the crystal.

It is worth noting that the determination of the distribution of magnetization remains an unresolved problem in the general case - usually not determined in the case of magnetization distribution of noncollinear systems.

In this paper it was shown how in a simple manner - using the general knowledge of the distribution of magnetic moments in the unit cell of the crystal - the vectorial magnetization distribution can be determined. It has been shown that the magnetic structure factors can be expressed as the combination of the “partial” magnetic structure factors. Each partial structure factor depends on different component of magnetic moments of the atom in the system. From the other hand, the same set of these “partial” magnetic structure factors can be expressed as the functions of the internal magnetization distribution. Once the set of these “partial” structure factors was obtained, the Maximum Entropy Method can be easily applied and the distribution of the magnetization in the noncollinear magnetic system can be fully reconstructed.

11 MAIN ACHIEVEMENTS

The polycrystalline $\text{Sc}_{0.946}\text{Fe}_{3.934}\text{Al}_8$ discloses $q_{xy} = (0.136(2), 0.136(2), 0)$ modulation which does not change with temperature up to 175 K [**H1**]. The aluminum atoms stabilize the crystal structure and since have almost zero magnetic moment, do not influence essential magnetic properties of the system. The iron atoms carry magnetic moment of $1.08(12) \mu_B$, while scandium ones are treated as non-participating in the formation of the magnetic structure. The spins of the iron atoms form a flat spiral in the basal ab plane rotating by $49(1)^\circ$ from cell to cell. The angle of rotation, $\frac{\pi}{4}$, perfectly explains the lack of any Zeeman sextets’s asymmetry, observed at 12 K, measured by polarized radiation, indicating a strong antiferromagnetic coupling without any ferromagnetic component.

Single crystal of ScFe_4Al_8 reveals the presence of a magnetic modulation $\vec{q}_1 = (\pm 0.13, \pm 0.13, 0)$, but much more magnetic reflections associated with modulation $\vec{q}_2 = (\pm 0.18, \pm 0.18, 0)$ were collected [**H2**, **H3**]. In light of these results the simplest expected magnetic structure seems to be a double cycloid spiral. According to LT neutron measurements the two magnetic modulations are comparatively strong. Analysis of the magnetism around iron atoms in scandium alloy shows that within the first few coordination zones (of width of about 0.1 \AA) the magnetic atoms are present only in I^{st} , III^{rd} and V^{th}

coordination zones around the selected iron atom position. Further on it was shown that at a distance not exceeding the shorter lattice parameter the atoms with magnetic moments are far away from each other. The scandium atoms similarly to weakly magnetic or ‘nonmagnetic’ Actinides occupying II and IV zones can participate in magnetic interactions by superexchange or polarization mechanism, which would facilitate and partly enhance the magnetic modulation along [110] direction. No similar effect is observed along the direction of $[\bar{1}10]$, and therefore the exchange interactions along this direction must be governed by other rules. The phase transition temperatures observed for the single crystal in the temperature range 5 – 250 K indicate a possibility of creating two subsystems of magnetic moments forming different magnetic structures: one antiferromagnetic and the other one described as weak ferromagnetism. In addition, these structures clearly exhibit different thermal dynamic: the q_1 modulations exists below 220 K while the modulation with q_2 exists below 130 K. Weakly ferromagnetic nature of system is associated with modulation $\vec{q}_2 = (\pm 0.18, 0.18, 0)$. The presence of magnetic domains is a factor masking here system's ferromagnetism. In the case of modulation $\vec{q}_1 = (\pm 0.13, 0.13, 0)$ no satellite reflections were observed around the nuclear $(2n\ 2n\ 2n)$ ones, which however does not show that one deals with a simple ferromagnetic material. The model calculations of magnetic structure factors indicates for phase difference in the different magnetic domains about $\pi/2$. However, consequence of this condition was calculated magnetic almost twice smaller than the experimental magnetic moment of the iron atom.

The spots localized at the Laue photograph, which are not indexed within body centered cell $(a \times a \times c)$ require larger unit cell dimensions [H4]. The observed vanishing of the spots above a temperature of 100 K leaves no doubt that the satellites are related to the modulation previously described as \vec{q}_2 . However, the results obtained by means of a Laue technique cannot exclude the participation of the modulation type \vec{q}_1 . Just because of other extinctions rules, magnetic satellites type \vec{q}_1 occur only around the reflection type $(2n + 1, 2n + 1, 2n)$ and not around $(2n, 2n, 2n)$ like for example $(\bar{2}00)$. A folding of the unit cell, keeping its tetragonal body-centered character, but with a doubling of the three cell parameters $(2a \times 2a \times 2c)$ allowed to completely simulate of the experimental diffraction patterns. Unfortunately, there is also another unit-cell and symmetry, which can describe Laue's data equally well, namely an orthorhombic primitive unit cell with the dimensions: $(2a \times a \times 2c)$. The neutron experiment carried out on VIVALDI turned out to be inconclusive with regard to the exact determination of the general crystal structure. Thanks to a Laue hard X-ray test, using an energy (100 – 400 keV dispersive technique), two intense Bragg reflections were measured at low diffraction angles. They correspond to the (200) and (310) reflections. However, in both cases, two weak but significant additional reflections were observed at low energy. They correspond to longer d -spacing, forbidden with the I symmetry: $(a \times a \times c)$ of unit cell, but which can be easily explained by a cell doubling along both a and b directions. Because of the

equatorial geometry of the diffraction experiment, this technique cannot afford information about the c direction.

In a $\text{Sc}_{1+x}\text{Fe}_{4-x}\text{Al}_8$, $x=0.1$ sample with a trace of $\text{Fe}_4\text{Al}_{13}$ extra phase SEM, XRD and ND measurements confirmed excess concentration of Sc, which locates in the $(8f)$ positions as expected, without destroying the magnetic order [**H5**]. A double cycloid disclosed slightly smaller modulation $\vec{q} = (\pm 0.131(2), 0.131(2), 0)$ with respect to that one obtained for stoichiometric scandium sample and the output rearrangement of the magnetic iron moments inclined by an angle of $\alpha \cong \frac{\pi}{12}$ relative to direction $[110]$. The competition of exchange interactions leads to noncollinear arrangement of magnetic moments of iron at sublattice $(8f)$. If it is taken as a first type of system's noncollinearity (intra-sublattice) in the case of excess scandium contribution decreases slightly modulation vector of the magnetic structure. This is accompanied by approximately 30% decrease of the Fe magnetic moment in comparison to the value of $1.23(6) \mu_B/\text{atom}$ and $1.19(8) \mu_B/\text{atom}$, depending on the domains in the ideal stoichiometric single crystal. Comparing the polycrystalline samples only, about 20% decrease of Fe magnetic moment from $1.08(12) \mu_B/\text{atom}$ in sample with about 5% deficiency of scandium to $0.87(4) \mu_B/\text{atom}$ in sample with about 10% excess concentration of scandium was obtained. The type of neighbor occupying (2a) does not substantially affect the canting angle of iron spins.

Consistent description of the experimental data was found within the model of spin-orbit coupling (SO), the $RKKY$ – type interactions and anisotropic Dzyaloshinskii–Moriya (DM) [**H6**]. It was not surprising to find twice as small exchange interaction along the c -direction in the crystal containing scandium compared to the corresponding exchange interaction of rutile structure, where the distances of magnetic nearest neighbors are much smaller (~ 150 pm). Similarly, its positive sign is not surprising, because usually the magnetic moments of atoms in MFe_4Al_8 systems are oriented ferromagnetically along this direction. It is worth noting that the oscillatory sequence of exchange integrals along the a -direction clearly indicate for $RKKY$ type of interaction. Participation of scandium ions in the sample magnetism is not excluded and may contribute to the combination of anisotropy of DM type or of the dipol – dipol interaction origin. It was verified that the magnetic moment of scandium between zero and $0.023 \mu_B$ along the $[010]$ does not lead to changes in the characteristics of magnetization at low temperatures. The collinear ferromagnetism is commensurate with the positions (2a) as in UFe_4Al_8 was assumed in Monte Carlo calculations. The simplicity of the proposed description, obtained map of interactions encourages further investigations.

Calculation by using $MCPPhase$ carried out on the base of $RKKY$ and DM interactions [**H7**] result in substantially weaker anisotropic interaction with respect to the one obtained, based on the obtained experimentally magnetic moment of iron of $1.38 \mu_B/\text{atom}$. This moment is stable up to $T = 11$ K and leads to overestimated intensities of the neutron reflections. On

the other hand, calculations within the *MCMag* indicate in most of cases the weaker exchange interactions but faithfully reproduce the resultant magnetic moment $1 \mu_B/\text{atom}$ of Fe which is stable up to $T = 51 \text{ K}$. Regardless of the calculation method, treating the spins quantum - mechanically or classically, has led to a satisfactory description of the experimental results. Maps of exchange integrals have been reconstructed.

In the case of a system containing uranium - doubly noncollinear - the values of canting angle was considered in terms of the exchange integrals ratios [H8]. Successful reconstruction the spin arrangement based on exchange integrals and phase transition temperatures at a level of commensurate structure or with a single modulation was achieved. Consistently with experimental results, one does not observe the lowering of resultant moments on the iron atom below $0.87 \mu_B$ and $1.46 \mu_B$, respectively. However the compatibility of the relationship of the obtained exchange integrals is much worse: $-1.2_{MCMag} > \frac{J_{aa}}{J_{bb}} > -1.8_{MCPHase}$ and $-67_{MCMag} < \frac{J_{aa}}{J_{cc}} < -2.5_{MCPHase}$. The Monte Carlo calculations indicate for the strongest exchange interaction along *a*-direction and of a different type than along the other two orthogonal directions. The weakest exchange interactions can be seen in the *c*-direction. Particularly weak interactions J_{cc} i.e. about 67 times fainter in relation to dominating J_{aa} were obtained in the course of calculations using *MCMag* package. In contrast, the relationship of J_{aa} to J_{bb} are comparable in absolute values (according *MCMag*) although at the direction of *b* are almost twice weaker compared to the strongest exchange constants (by *MCPHase*). This result agrees poorly with the experiment range of accepted values of canting angle. Namely, stable spin-canted structure is provided for canting angles in the range of $\pi/5 < \alpha \leq \pi/2$, while the results of experiments indicate on the canting angle $\alpha \leq \pi/6$. The strongest coherent neutron scattering was observed along the diagonal [110] which leads to expectations of positive signs of integrals J_{ac}, J_{abc} . While the relationship $J_{aa} = -J_{bb}$ without doubt stems from *DM* anisotropy.

A set of "partial" structure factors - depending on the various components of the magnetic moment of the atom - allows for full reconstruction of the internal magnetization distribution by the use of the maximum entropy method [H9]. This type of analysis of rarely carried out in the literature on noncollinear systems.

Presented analysis relates to noncollinear and/or incommensurate magnetic structures revealed under conditions of weak diffraction intensities.

Bibliography

- 1ⁱ P.W. Anderson, *Science, New Series*, Vol.177, No.4047 (1972) 393
- 2ⁱⁱ P. Schobinger-Papamantellos, K. H. J. Buschow, C. Ritter, *J. Magn. Magn. Mat.* 186 (1998) 21
- 3ⁱⁱⁱ W. Sikora, P. Schobinger-Papamantellos, K.H.J. Buschow, *J. Magn. Magn. Mat.* 213 (2000) 143
- 4^{iv} K. H. J. Buschow, *Rep. Prog. Phys.* 54 (1991) 1123
- 5^v D X Li and Yshiokawa, *J. Phys.: Condens. Matter* 15 (2003) 2029
- 6^{vi} H.H. Hill, *Plutonium 1970 and other Actinides*, Eds. W.N. Miner, Metal Soc. AIME, New York, 1970, p.2
- 7^{vii} K. Rećko, K. Szymański, L. Dobrzyński, D. Satuła, B.C. Hauback, W. Suski, B.Yu. Kotur, *Molecular Physics Reports* 38 (2003) 113
- 8^{viii} J.A. Paixão, B. Lebech, A.P. Gonçalves, P.J. Brown, G.H. Lander, P. Burlet, A. Delapalme, J.C. Spirlet, *Phys. Rev. B* 55 (1997) 14370
- 9^{ix} K. Rećko, M. Biernacka, L. Dobrzyński, K. Perzyńska, D. Satuła, J. Waliszewski, W. Suski, K. Wochowski, G. André, F. Bourée, *J. Phys. Cond. Matter* 9 (1997) 9541
- 10^x W.Sikora, F.Białas and L.Pytlik - MODY: a program for calculation of symmetry-adapted functions for ordered structures in crystals, *Journal of Applied Crystallography*, 37(2004), 1015-1019
- 11^{xi} J. Rodríguez-Carvajal, Recent advances in magnetic structure determination by neutron powder diffraction, *Physica B* 192 (1993) 55-59
- 12^{xii} Petricek V, Dusek M and Palatinus L 2006 *Jana 2006: The Crystallographic Computing System* (Prague: Institute of Physics)
- 13^{xiii} <http://www.cryst.ehu.es> (Bilbao Crystallographic Server)
- 14^{xiv} F. Sayetat, P. Fertey, M.J. Kessler, *Appl. Cryst.* 31 (1998) 121
- 15^{xv} H. Iwanga, A. Kunishige, S. Takeuchi, *J. Mater. Sci.* 35 (2000) 2451
- 16^{xvi} S. Kirkpatrick, C.D. Gellatt Jr I M.P. Vecchi, *Science* 220 (1983) 671
- 17^{xvii} N. Metropolis A.W. Rosenbluth, M.N.Rosenbluth, A.H. Teller I E. Teller, *J. Chem. Fiz.* 21 (1953) 1087
- 18^{xviii} O. Nabuhiko, H. Yoshikazu, *J. Phys. Soc. Jpn.* 30 (1971) 1311
- 19^{xix} P. Hohenberg and W. Kohn: *Inhomogeneous Electron Gas*. *Phys. Rev.* 136 (1964) B864-B871
- 20^{xx} H. Bruning, PhD thesis. University of Twente Enschede (1992), The Netherlands
- 21^{xxi} R.Y. DeVries, PhD thesis. University of Twente Enschede (1996), The Netherlands

